Chapter II

Know Mother Best: Measurement and Modeling of the Properties of the Mother Phase Relevant to Bubble Nucleation

> If we want to understand the birth and growth of the baby, we ought to get to know its mother.
>
> Prof. Julie Kornfield

A.Y. and Prof. Ernesto Di Maio measured polyol–CO_2 properties with G-ADSA in the Di Maio lab at the University of Naples Federico II with initial help from Dr. Maria Rosaria Di Caprio. Dr. Jacob Crosthwaite measured the solubility of VORANOL 360 at Dow, Inc., Midland, MI. Dr. Huikuan Chao developed the theoretical models, which A.Y. fit to the data.

Try as a bubble might to be independent, it will always depend on its mother phase, the medium from which it nucleates. A bubble cannot exist unless its mother phase has a sufficient excess of dissolved gas to give it birth. A bubble cannot survive unless it overcomes the tension along the interface dividing it from its mother phase. A bubble cannot grow unless it receives gas by diffusion from its mother phase.

Any prediction of a bubble's life in a polymer foam requires knowledge of the gas solubility, interfacial tension, and gas diffusivity in the polymer component of its mother phase. In this Chapter, we describe a method to measure these key physical properties for our polyurethane model system, carbon dioxide in a polyether polyol. We close by fitting a thermodynamic model of the polyol–CO_2 mother phase to the measured properties.

Because these properties are interdependent, they must be measured simultaneously. The simultaneous measurement of these properties for binary gas–polymer mixtures is possible with gravimetry–axisymmetric drop shape analysis (G-ADSA)[1], a technique pioneered by Prof. Ernesto Di Maio, who permitted the use of his custom instrument at the University of Naples Federico II for the present work. We describe the method and analysis in Section II.1.

Because a high supersaturation of CO_2 is necessary to observe homogeneous bubble nucleation in our microfluidic channel, we pay specific attention to the types of polymer architectures that maximize the CO_2 solubility in Section II.3. The solubility of CO_2 in polyol has additional applications in the foaming industry. While CO_2 in polyurethane foams is typically produced *in situ* by chemical blowing, the equilibrium CO_2 solubility can still affect foaming [2]. Additionally, a high equilibrium CO_2 solubility is required in alternative polyurethane foaming processes that utilize pre-dissolved CO_2 in the polyol and isocyanate to achieve desired structures and minimize polyurea formation inherent in foams wherein CO_2 is formed through water-blowing, which can compromise strength, stiffness and processability [3–5]. Previous studies have suggested that maximal solubility of polyol in CO_2 balances the entropic penalty of a longer molecular weight with the enthalpic gain of a higher ratio of ether to hydroxyl end groups [4], but this trend has not been demonstrated for CO_2 solubility in polyether polyols, the focus of the present work. This trend is important to guide the selection of the structure of polyols used in polyurethane foaming to achieve desired structural characteristics and, ultimately, desired thermal and mechanical properties in CO_2-based polyurethane foams.

Currently, the effect of the molecular structure of the polyol on CO_2 solubility remains unclear due to conflicting trends reported as a function of molecular weight and hydroxyl functionality. We reconcile these conflicting reports of CO_2 solubility in polyether polyols through experiments that isolate the effects of molecular weight and hydroxyl functionality. We show that CO_2 solubility decreases with molecular weight above 1000 g/mol due to reduced mixing entropy and decreases with hydroxyl functionality due to increased concentration of CO_2-phobic, self-preferential hydrogen bonds. The competition between these trends explains the increase in CO_2 solubility with molecular weight for short polyols (less than 1000 g/mol), validated by the available literature. Due to the importance of hydrogen bonds in governing CO_2 solubility, below 1000 g/mol, an accurate PC-SAFT model will likely need to account for the associative hydrogen-bonding interactions among the hydroxyl groups. These results led us to select polyether polyols with 2–3 hydroxyl groups per polymer and an intermediate molecular weight (1000 g/mol) for maximal CO_2 solubility.

We further use the measurements from G-ADSA to fit parameters of a thermodynamic model of these mixtures based on the perturbed chain–statistical associating fluid theory (PC-SAFT) described in Section II.4. This model serves

two purposes: first, it allows us to estimate the properties of polyol–CO_2 mixtures that we produce in the lab and, second, it serves as the foundation of additional models of the interface, bubble growth, and bubble nucleation. We briefly describe the use of a classical density functional theory (DFT) based on the PC-SAFT model for modeling the interface between the polyol-rich and CO_2-rich phases in Section II.4. We explore the role of these models in the prediction of bubble growth in Chapter V and of nucleation in Chapter VI.

II.1 Gravimetry–Axisymmetric Drop Shape Analysis (G-ADSA) Measures Physical Properties of Polyol–CO_2 Mixtures

Gravimetry–Axisymmetric Drop Shape Analysis (G-ADSA) [1] is a technique for simultaneous measurement of the properties of liquid–gas mixtures that combines weight measurements using a magnetic suspension balance (gravimetry) with pendant drop analysis (axisymmetric drop shape analysis). Its measurements can be used to estimate gas solubility, specific volume, gas diffusivity, and interfacial tension. In the present work, we employed this technique to measure these properties for mixtures of CO_2 and polyether polyols of various molecular weights and functionalities (see Table II.1) in the range of 0–8 MPa at 30 °C and 60 °C. Here, we briefly describe the apparatus and technique. For a more thorough discussion, we refer the reader to the original publication of this method by Pastore Carbone *et al.* [1].

Name	M_n (g/mol)	f	ρ (g/mL)	η (mPa.s)	Supplier
1k2f	1000	2	1.02	160	Dow, Inc.
1k3f	1000	3	1.02	290	Dow, Inc.
1k5f	728	4.7	1.084	4820	Dow, Inc.
3k2f	2700	2	1.004	740	MilliporeSigma

Table II.1: Table of properties of the polyols used in this study (M_n = number-averaged molecular weight, f = functionality or number of hydroxyl groups per chain, ρ = density, η = viscosity). Values reported are averages. Molecular weights, functionalities, and densities supplied by manufacturers. Viscosities measured using ARES shear rheometer. Density and viscosity measurements measured at 25 °C. Polydispersities are not known.

Apparatus

Briefly, a magnetic suspension balance (MSB, Rubotherm Prazisionsmesstechnik GmbH, Germany) holds a Pyrex crucible with an inner diameter of 1.82 cm that contains the polyol sample. The crucible is suspended from the MSB by hooks with

a volume of 2.26735 mL, as measured in a helium atmosphere by Dr. Maria Rosaria Di Caprio of the Di Maio lab [1]. A Teflon rod with a diameter of 2.05 mm is fitted snugly into a slot in the apparatus to hold the pendant drop. The MSB is encased in a steel high-pressure cell, which is sealed around the MSB with a rubber O-ring. Two sapphire windows of a few centimeters in diameter machined in the cell provide a clear view of the pendant drop to a video camera with a convex objective lens.

Method

Before each measurement, an analytical balance was tared with the crucible. 1 mL of the desired polyol was then slowly poured into the crucible, taking care not to entrain any bubbles, and the weight of the sample under normal temperature and pressure was measured with the MSB. Next, to prepare the pendant drop, a drop of polyol was first deposited onto the corner of a clean glass slide. The corner of the slide was then tilted over the upward-facing tip of the Teflon rod until a small drop (3–5 μL) dripped off and formed a hemisphere atop the tip of the rod. The rod was then inverted carefully to prevent loss of the drop and inserted into a slot in the MSB. The high-pressure steel encasement was then sealed around the MSB gently enough that the pendant drop would not fall. The high-pressure cell was enveloped in a second stainless steel jacket, which contained oil that was heated with a heating circulator (Julabo F25) to control the temperature of the sample. Once sealed, the pressure of CO_2 inside the high-pressure cell was controlled using a Belsorp system. During the first stage of each experiment, moisture was removed from the polyol sample and the pendant drop by pulling a vacuum until the sample weight stopped decreasing. If the sample weight did not stop decreasing within 15–20 minutes, we assumed that the additional mass loss resulted from the loss of the polyol, which could contain some polymer chains small enough to be slightly volatile. At this point, the weight of the pure polyol sample and the volume of the pure polyol pendant drop were measured.

The measurement of the pure polyol sample was followed by several measurements after pressurization with CO_2. Pressurization was performed using the Belsorp system to slowly inject CO_2 into the chamber. Above 5500 kPa, the Belsorp could not supply sufficient CO_2 pressure to pressurize the chamber further, so we used an ISCO pump to pressurize the CO_2 first before injecting it manually. Throughout each measurement, the MSB recorded the changing mass of the crucible as CO_2 was absorbed into the polyol. The pressure was kept constant (within 20 kPa) until the mass did not change by more than 30 μg in five minutes. At this point,

we considered the system to be sufficiently close to equilibrium for the error to be negligible. Upon reaching equilibrium, the MSB lowered the crucible until it rested on an overhanging platform, allowing the MSB to take three measurements of the tare weight. At the same time, a video camera captured images of the pendant drop as it swelled from absorption of CO_2, which were taken every few minutes. The Teflon rod swelled as well, as shown in Figure II.S1 of the Supporting Information (SI). These measurements were repeated at ever higher pressures until reaching the maximum pressure for the experiment between 5–8 MPa. At this point, we depressurized the system in steps by releasing CO_2 through an automated ball valve from the high-pressure cell, taking measurements at each step. The release of CO_2 was performed slowly enough that no nucleation of bubbles was observed in the pendant drop. Overall, we took measurements at 10–20 pressure values over the course of 1 week for each set of conditions.

Compute Gas Solubility, Specific Volume, Gas Diffusivity, and Interfacial Tension from G-ADSA Measurements

The G-ADSA technique only directly measures an image of the drop shape, the total apparent weight of the crucible, attaching hooks, and sample, and the apparent weight of the tare. The specific volume of the polyol–CO_2 mixture, solubility of CO_2 in the polyol, diffusivity of CO_2 in the polyol, and interfacial tension between the polyol-rich and CO_2-rich phases must therefore be calculated from these raw data. These calculations were performed with custom methods using open-souce Python packages, including jupyter[6], matplotlib [7], numpy [8], pandas [9], and scipy [10]. The corresponding notebooks and libraries can be found in the GitHub repository `andylitalo/g-adsa` [11].

The general scheme of these calculations is summarized here. For further detail, we refer the reader to the Supporting Information (SI).

We first estimated the equilibrium volume of the pendant drop from the shape of the pendant drop using the commercial software FTA32 (First Ten Angstroms). We then estimate the sample volume by assuming that its volume changes proportionally to the equilibrium volume of the drop. Next, we estimated the equilibrium sample mass using the MSB. The balance only directly measures the apparent weight and the tare weight. The difference between these measurements gives the sum of the masses of the sample, the crucible, and the supporting hooks minus the effect of the buoyant force, which must be accounted for due to the precision of these

measurements. To compute the buoyant force, we multiply the density of CO_2 at the given pressure and temperature (available on the NIST Chemistry WebBook [12]) by the total volume of weighed objects, which includes the volumes of the crucible, the supporting hooks, and the sample. The volume of the crucible and hooks was previously measured by Dr. Maria Rosaria Di Caprio in a helium atmosphere [1]. After correcting for buoyancy effects, the difference between the balance readings for the apparent weight and tare weight at zero pressure gives the mass of dissolved gas. We then estimated the dry mass of the polyol by pulling a vacuum to remove dissolved vapor and moisture. The CO_2 solubility is then the mass of dissolved gas divided by the total sample mass, equal to the sum of the mass of dissolved gas and the dry mass of the polyol. The specific volume of the sample can then be calculated by dividing the sample volume by the total sample mass.

To estimate the diffusivity, we followed the model derived by Crank for diffusion into a slab [13] and described in Section II.S1. The model considers an infinite slab of fluid with a concentration-dependent diffusivity and a gas atmosphere on both sides. In our case, the polyol sample is only open to the CO_2 atmosphere on one side. The situation is nevertheless analogous if we map the midpoint of the slab to the base of the crucible because there is no flux through either surface.

With this model, we can estimate the diffusivity of CO_2 as a function of the saturation pressure in the sample in two ways: (1) fit a square root function to the mass of dissolved gas over time at early times, and (2) fit an exponential function to the mass of dissolved gas over time upon approaching equilibrium. While we used both to estimate the diffusivity, we generally used the first method (square root) due to better fitting of the data and lower sensitivity to noise. In practice, because the concentration changes during the measurement of gas diffusivity, we can only measure an upper and lower bound at a given concentration. Our measurement of diffusivity after pressurizing provides the upper bound because the CO_2 concentration begins lower than the equilibrium value, and our measurement after depressurizing provides the lower bound because the CO_2 concentration begins higher than the equilibrium value.

Finally, we estimate the interfacial tension at a given pressure using axisymmetric drop shape analysis (ADSA) performed with the commercial software First Ten Angstroms 32 (FTA32). This software automatically detects the edge of the drop and fits the contour predicted for a pendant drop predicted to its shape. When provided the density of the drop (reciprocal of the specific volume) and the density of

the CO_2-rich atmosphere (estimated using the pvT data for pure CO_2 available from NIST [12]), the software computes the interfacial tension. To learn more about the pendant drop method and its estimation of interfacial tension, see the work of Song and Springer [14]. Because ADSA was performed using a camera separate from the Rubotherm MSB used for gravimetry, the two sets of measurements were synchronized to a common start time, thereby providing simultaneous measurements of each parameter. See Section II.S1 of the SI for further experimental details, analysis, and discussion of sources of error.

II.2 G-ADSA Measurements: Effects of Pressure and Temperature

Here, I will describe the effects of pressure and temperature on CO_2 solubility, specific volume of a polyol–CO_2 mixture, the interfacial tension between the polyol-rich and CO_2-rich phases, and the diffusivity of CO_2.

One key aspect governing the properties of polyol-CO_2 mixtures is whether the CO_2 is subcritical to supercritical. To explore this aspect, we show the solubility of CO_2 in polyol (difunctional, 1000 g/mol, supplied by Dow, Inc.) as a function of pressure for subcritical and supercritical temperatures in Figure II.1. In this figure, we combine data measured with G-ADSA in the Di Maio lab and data measured with a magnetic suspension balance (MSB) by Dr. Jacob Crosthwaite at Dow, Inc. (Midland, MI). The agreement between adsorption ($\circ$) and desorption ($\times$) measurements with G-ADSA and the agreement between G-ADSA in the Di Maio lab and MSB at Dow, Inc. at 60 °C testifies to the consistency of these measurement techniques. Therefore, although time limited the repetition of these week-long experiments, we believe their results are reproducible.

From the data, we see that the CO_2 solubility grows roughly linearly with pressure at low pressures (below 2000 kPa), as expected from Henry's law. As the pressure increases, the effect of temperature becomes more pronounced. If the temperature is subcritical (< 31 °C), the CO_2 solubility increases superlinearly, as observed for the data measured at 25 °C and at 30.5 °C. At high enough pressure, the CO_2 atmosphere eventually condenses into a liquid phase (> 6430 kPa at 25 °C [12]). This liquid atmosphere may dissolve a non-negligible amount of polyol and violate our assumption of a fixed polyol mass (see Section II.1), so measurements were not taken above 6000 kPa. At the supercritical temperature of 60 °C, however, the CO_2 solubility increases roughly linearly well above the critical pressure (7.38 MPa [12]), which is qualitatively consistent with solubility measurements for CO_2

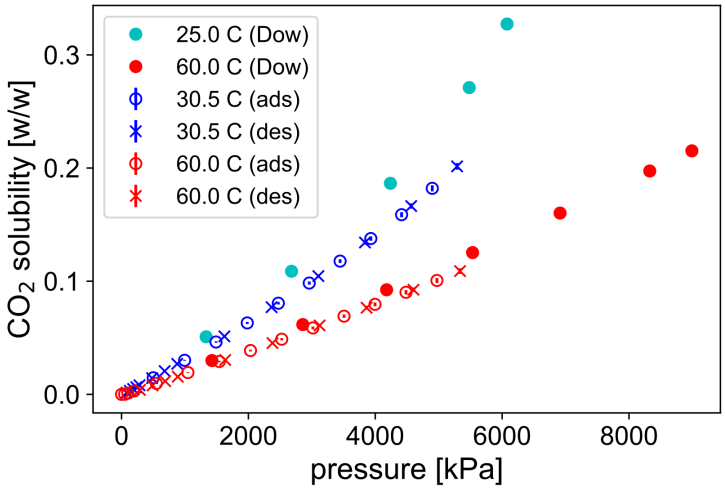

Figure II.1: CO_2 solubility in difunctional (two hydroxyls per chain), 1000 g/mol polyol as a function of pressure for different temperatures (indicated by color). Data are combined from G-ADSA measurements made with Prof. Ernesto Di Maio at the University of Naples Federico II (adsorption ∘ and desorption ×) and measurements made with an MSB at Dow, Inc. (Midland, MI) by Dr. Jacob Crosthwaite (•). Error bars are shown, but are sometimes smaller than the marker.

in polyols in the literature [2, 5, 15]. We expect the slope to decrease at a high enough pressure as observed above 10 MPa for CO_2 in PMMA [16].

We will return to CO_2 solubility to discuss the effects of polymer architecture in Section II.3, but now we turn to the effects of pressure and temperature on the other thermophysical properties measured by G-ADSA (specific volume, interfacial tension, and CO_2 diffusivity). Because the Julabo temperature controller available in the Di Maio lab for G-ADSA could only heat and not chill its silicone oil bath, its minimum temperature was limited to 30.5 °C by the ambient temperature (> 25 °C in the Naples summer) and the viscous heating caused by flow, so we could not directly repeat the measurements performed at Dow at 25 °C. Additionally, this temperature is within experimental uncertainty (0.5 °C) of the critical temperature for CO_2, 31 °C, so we cannot guarantee that the CO_2 at the lower temperature did not become supercritical during these measurements. To increase reproducibility, we will present data for a commercially available poly(propylene glycol) (average $M_n \approx 2700$ g/mol, MilliporeSigma, CAS 25322-69-4). In each dataset, data from two measurements performed at 60 °C are shown. They are indistinguishable from each other beyond statistical uncertainty, further demonstrating the reproducibility of the G-ADSA measurements.

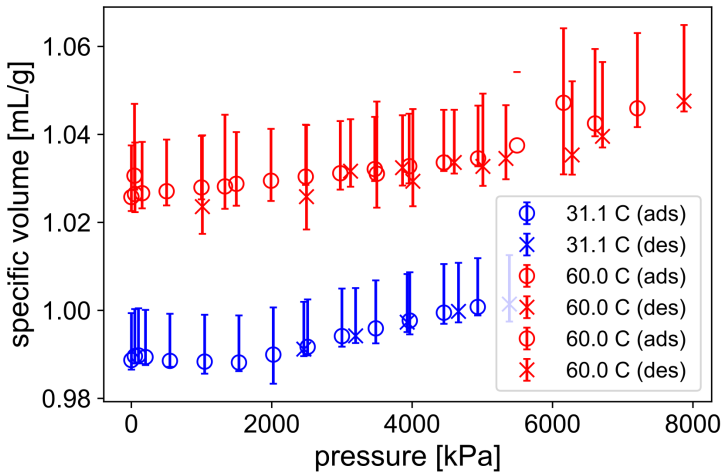

Figure II.2: The specific volume of a mixture of poly(propylene glycol) (PPG) of molecular weight 2700 g/mol and CO_2 as a function of pressure, measured with G-ADSA. Measurements were taken during both adsorption (○) and desorption (×) of CO_2 with agreement within uncertainty. Upper error bars indicate systematic error and lower error bars indicate statistical error. Data are shown at 31 °C (blue) and 60 °C (red). Data were collected in the lab of Prof. Ernesto Di Maio at the University of Naples Federico II.

The specific volume (reciprocal of the density) of the PPG–CO_2 mixture generally increased with pressure and temperature but exhibited a unique, non-monotonic behavior at low pressure and temperature. This behavior is shown in Figure II.2, where the specific volume at 31.1 °C slightly decreases with pressure from 0–1000 kPa before increasing steadily with further increase in pressure. While this small variation in the specific volume is much smaller than the systematic error (upper error bars), it is slightly larger than the statistical error (lower error bars), suggesting that it is not the result of noise. The Di Maio group has previously reported a similar non-monotonic dependence of the specific volume on pressure from measurements with G-ADSA for a formulation of polyether polyols [2] and for poly(caprolactone) (PCL) [17]. They further demonstrated that this behavior is the result of different packing densities of CO_2 in the polymer matrix at different pressures using evidence from Raman spectroscopy [18–20].

The interfacial tension between the polyol-rich and CO_2-rich phases decreased with pressure and decreased with temperature when the concentration of dissolved CO_2 was fixed. These two behaviors are shown in Figures II.3a and II.3b. The decrease in the interfacial tension with pressure seen in Figure II.3a is expected given that the CO_2-rich atmosphere becomes more similar in density to

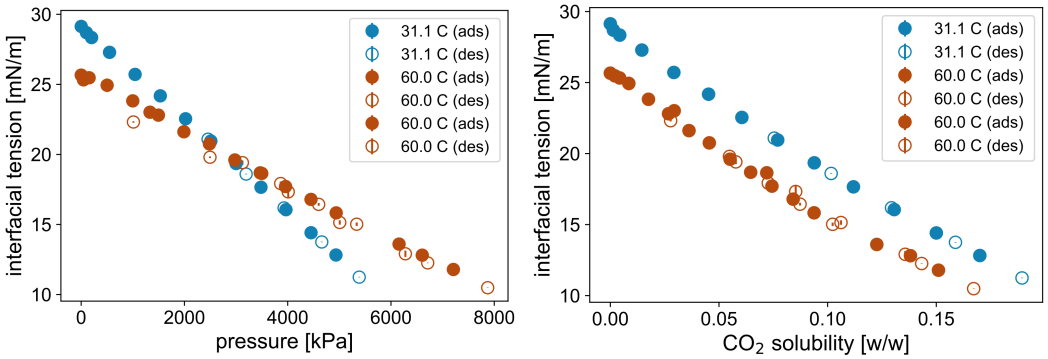

(a) Interfacial tension vs. pressure

(b) Interfacial tension vs. solubility

Figure II.3: Interfacial tension of a mixture of PPG and CO_2 between the polyol-rich and CO_2-rich phases G-ADSA. Measurements were taken during both pressurization (filled circles) and depressurization (empty circles) of CO_2 with agreement within uncertainty. Error bars shown but may be smaller than glyph for some data points. Data are shown at 31 °C (blue) and 60 °C (red). Data were collected in the lab of Prof. Ernesto Di Maio at the University of Naples Federico II.

the polyol-rich phase as the pressure increases, consistent with previous G-ADSA measurements from the Di Maio group for a formulation of polyether polyol [2] and PCL [17] and by Yang *et al.* for various polyols [5]. From this figure, we see that the effect of temperature depends on the pressure: at low pressure, interfacial tension decreases with temperature, but at high pressure, interfacial tension increases with temperature. The reason for this non-monotonic effect of temperature at different pressures is more clearly seen in Figure II.3b, where the interfacial tension is plotted as a function of the weight fraction of dissolved CO_2. Here, increasing the temperature decreases the interfacial tension, as is observed for pure liquids due to the increased entropic driving force for mixing. At a fixed pressure, however, increasing the temperature decreases the amount of dissolved CO_2, and the amount by which it decreases is greater at higher pressure (see Figure II.1). Because the interfacial tension decreases with the amount of dissolved CO_2 (due to the increased similarity of the polyol–CO_2 mixture to the CO_2 atmosphere), the reduction in dissolved CO_2 with temperature can increase the interfacial tension more than raising the temperature alone decreases it. The result is the increase in the interfacial tension with temperature at pressures above 3000 kPa. To our knowledge, measurements distinctly demonstrating this crossover in the interfacial tension with temperature have not been reported in the literature.

We observed that the diffusivity of CO_2 in polyol increased with pressure and temperature, consistent with previous measurements in other polyols [2, 5].

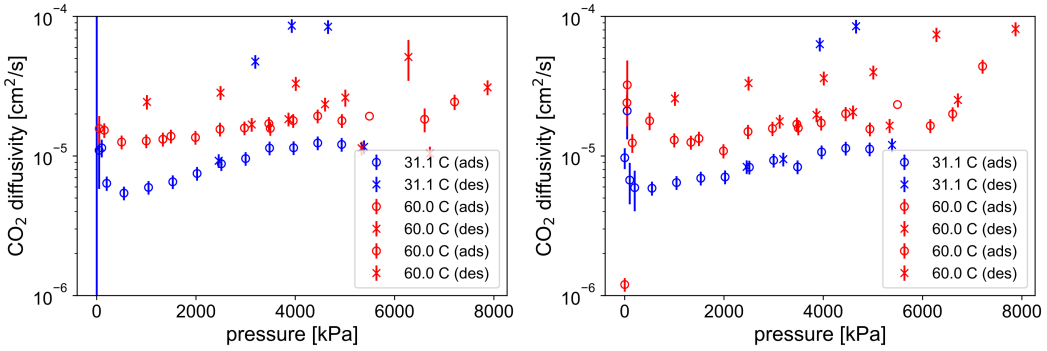

(a) Square-root fit method

(b) Exponential fit method

Figure II.4: The diffusivity of CO_2 in poly(propylene glycol) (PPG) of molecular weight 2700 g/mol estimated with the square-root fit (see Section II.1) as a function of pressure of CO_2 headspace, measured with G-ADSA. Measurements were taken during both adsorption ($\circ$) and desorption ($\times$) of CO_2 with agreement within uncertainty. Error bars may be smaller than glyphs of some data points. Data are shown at 31 °C (blue) and 60 °C (red). Data were collected in the lab of Prof. Ernesto Di Maio at the University of Naples Federico II.

Our estimation of the diffusivity from G-ADSA measurements is shown in Figure II.4 for the square-root fit method (II.4a) and the exponential fit method (II.4b) (see Section II.1 for details of these methods). While we expect a higher estimate of the diffusivity during desorption than adsorption, the difference should not be much larger than the difference in diffusivity over a similar pressure range. Our estimates yielded significantly higher diffusivities from desorption measurements, however, which we believe may be the result of depressurizing too quickly. Although increasing the temperature reduces the weight fraction of dissolved CO_2 (Figure II.1), which we observe decreases the diffusivity, the greater thermal energy conferred to the mixture at higher temperature appears to dominate that effect, leading to a monotonic increase in diffusivity with temperature, unlike the effect of temperature on interfacial tension (Figure II.3).

Finally, we compared our measurements with G-ADSA to measurements performed with other techniques. While our measurements with G-ADSA quantitatively agreed with those of the MSB reported by Dow, they significantly disagreed quantitatively with others reported in the literature [5, 15]. For a discussion of these comparisons, see Section II.S3 in the SI.

II.3 Discussion: Competition Between CO_2-philicity and Mixing Entropy Underlies CO_2 Solubility Maximum in Polyether Polyols

Because the solubility of CO_2 in a polymer profoundly shapes the structure and, consequently, the physical properties of CO_2-blown polymer foams, we direct specific attention to its dependence on polymer architecture in this section. The effect of the architecture of the polyol has not been systematically studied in full. Parks and Beckman provided useful intuition for the effect of polyol architecture on CO_2–polyol interactions in their study of the solubility of polyol in CO_2 [4]. They noted that because the carbon in CO_2 has a lower electron density, it has a strong attraction to the relatively electron-rich ether groups along the polyol backbone, which has since been demonstrated with quantum mechanical calculations [21]. In contrast, they reasoned that the CO_2-phobicity hydroxyl groups, caused by their preference for self-interaction by hydrogen bonding [21], would significantly decrease the solubility of short-chain polyols in CO_2, such as those used in polyurethane synthesis, due to the high proportion of hydroxyl end groups to ether groups along the backbone [4]. They ultimately found that the solubility of polyol in CO_2 increases with molecular weight for short chains, but decreases with molecular weight for longer chains as the decrease in the entropy of mixing with molecular weight dominates the enthalpic gain of a higher ratio of ether to hydroxyl end groups.

Indeed, Daneshvar *et al.* [22] and Li *et al.* [23] showed that the solubility of CO_2 in poly(ethylene glycol) (PEG) increases with molecular weight for short chains (150–1000 g/mol), as did Yang *et al.* for various polyether polyols in the range of 255–1000 g/mol [5]. Weidner *et al.* and Wiesmet *et al.* published measurements of CO_2 solubility in longer PEG chains of 1500–8000 g/mol at temperatures between 50–100 °C, but observed no statistically significant effect of molecular weight. Based on the work of Parks and Beckman and intuition from the Flory–Huggins model, we hypothesize that the solubility of CO_2 should decrease with molecular weight for long chains due to the decreased entropic gain from mixing. This effect will become more pronounced at lower temperatures and may be discernible with more precise measurements made possible with G-ADSA. To our knowledge, however, this trend has not been demonstrated with experimental measurements in the literature.

The effect of the number of hydroxyl groups per chain, known as the "functionality," was investigated by Yang *et al.*, who reported maximal CO_2 solubility in polyether polyols with 3 hydroxyl groups per chain [5]. This finding conflicts with the reasoning of Beckman and Parks that a higher concentration of hydroxyl

groups should reduce the attraction of CO_2 to polyol, so further study is in order. Uncovering these trends is important to guide the selection of the structure of polyols used in polyurethane foaming to optimize CO_2 solubility and achieve the desired thermal and mechanical properties in CO_2-blown polyurethane foams.

In the present study, we systematically investigate the effect of molecular weight and hydroxyl groups per chain on the solubility of CO_2 in polyether polyols. We measure the solubility of CO_2 using gravimetry–axisymetric drop-shape analysis (G-ADSA), which measures the change in mass of a sample upon absorption of CO_2 using a magnetic suspension balance while simultaneously measuring the specific volume for precise accounting of the buoyant force. Given the abundance of previous measurements of CO_2 solubility in polyols with a molecular weight smaller than 1000 g/mol, we selected longer polyols of 1000 and 2700 g/mol. Rather than observe the CO_2 solubility increase further with molecular weight, as reported in the literature for shorter polyols, we hypothesized that we would observe a decrease in CO_2 solubility with molecular weight, consistent with the observations of Parks and Beckman for the solubility of polyol in CO_2 [4]. We also systematically varied the average number of hydroxyl groups per chain from 2 to 4.7. Combined with the literature, these measurements reveal a non-monotonic dependence of the CO_2 solubility on molecular weight, peaking around 1000 g/mol, and a monotonic decrease with hydroxyl groups per chain.

We further use the measurements from G-ADSA to fit parameters of a thermodynamic model of these mixtures based on perturbed chain–statistical associating fluid theory (PC-SAFT) described in Section II.4. This model serves two purposes: first, it provides a general method for estimating the properties of polyol–CO_2 mixtures and, second, it can provide the foundation of additional models of the interface, bubble growth, and bubble nucleation. In the same section, we also briefly describe the use of a classical density functional theory (DFT) based on the free energy of the PC-SAFT model for modeling the interface between the polyol-rich and CO_2-rich phases, which we validate against interfacial tension measurements provided by G-ADSA. While the models accurately capture the CO_2 solubility and interfacial tension, the PC-SAFT model significantly underestimates the specific volume of the polyol-rich phase, likely because it does not account for associative interactions like hydrogen bonding. For polyols smaller than 1000 g/mol, an accurate PC-SAFT model even of CO_2 solubility may likewise require accounting for hydrogen bonding through associative interactions. Nevertheless, this study shows that CO_2 is most

soluble in polyether polyols of 1000 g/mol with as few hydroxyl groups as possible.

To explore the effect of polymer architecture on the amount of CO_2 it can dissolve, we separately studied the effects of hydroxyls per chain and the molecular weight, starting with the hydroxyls per chain. To our knowledge, investigation of the effect of the hydroxyl number per chain with a fixed molecular weight has not been previously reported in the literature. We considered the solubility of CO_2 of two polyols and a blend of polyol with a molecular weight of 1000 g/mol and different average numbers of hydroxyls per chain in Figure II.5. At low pressures, the difference in solubility is within the experimental uncertainty. At the higher temperature (60 °C, lower cluster of measurements) and at pressures above 3000 kPa, we can see that the polyol blend with the higher average number of hydroxyls per chain (4.7) has a significantly lower solubility of CO_2 than the other polyols; above 4000 kPa, the polyol with the middle average number of hydroxyls per chain (3) has a significantly lower solubility than the polyol with the fewest (2). This observation suggests that increasing the number of hydroxyls per chain decreases the solubility, with the difference becoming more apparent at higher pressures. This difference is less clear at the lower temperature data (upper cluster of measurements), in part because the CO_2 solubility in the polyol blend with an average of 4.7 hydroxyls per chain was measured at a lower temperature (25 °C) than the others (30.5 °C), yielding a higher solubility. While we cannot make this conclusion without measuring the CO_2 solubility at 30.5 °C and showing significantly lower values, we expect this to be the case based on a rough estimation of the effects of lower molecular weight and lower temperature on the solubility of CO_2, whose details are presented in Section II.S2 of the SI. Our observation of decreased CO_2 solubility with hydroxyl number per chain is consistent with the favorability of CO_2–ether interactions over CO_2–hydroxyl interactions [4, 21].

Next, we considered the effect of molecular weight on CO_2 solubility at a fixed hydroxyl number per chain of 2. We performed G-ADSA measurements of CO_2 solubility in two such polyols, one of 1000 g/mol and the other of 2700 g/mol, as shown in Figure II.6. The difference in solubility was not statistically significant at the higher temperature (60 °C, lower cluster of data), but the solubility was slightly lower for the longer polyol at the lower temperature (30.5–31.1 °C, upper cluster of data). The solubility of the longer polyol, however, was measured at a slightly higher temperature than that of the shorter polyol (31.1 °C for the longer vs. 30.5 °C for the shorter), which could have also led to the lower measurement of solubility.

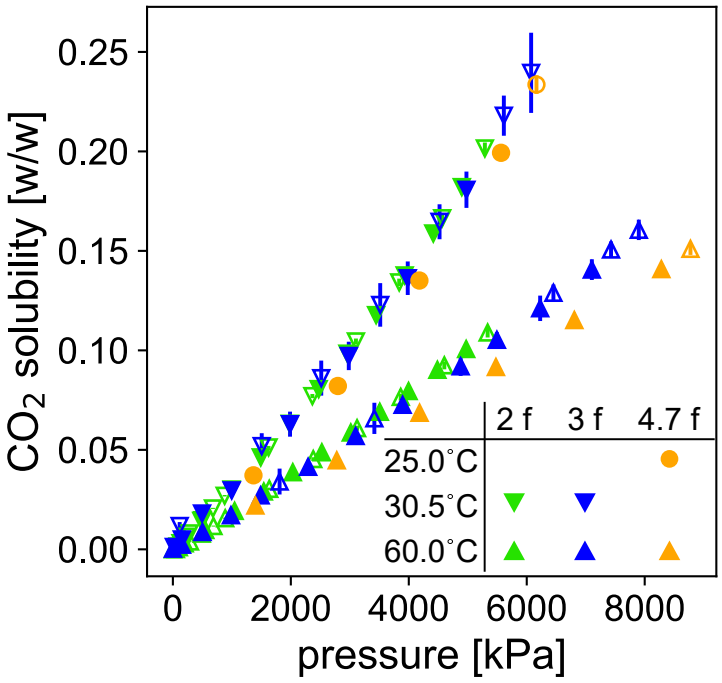

Figure II.5: The solubility of CO_2 in polyol as a function of pressure (measured with G-ADSA) is shown for polyols of three functionalities (average number of hydroxyl groups per chain): 2 (green), 3 (blue), and 4.7 (yellow) (labeled as "#f" in the legend). Each polyol has an average molecular weight of 1000 g/mol, except for the polyol with a functionality of 4.7, which has an average molecular weight of 728 g/mol (this effect is roughly cancelled out by the lower temperature). Measurements were taken during both pressurization (filled symbols) and depressurization (open symbols) of CO_2 with agreement within uncertainty. Error bars may be smaller than glyphs of some data points. Data are shown in two temperature clusters: the upper cluster contains data measured at 30.5 °C (downward triangle) for 2f and 3f but 25 °C (circle) for 4.7f; the lower cluster contains data measured at 60 °C (upward triangle).

Because our measurements are not sufficient to draw a clear conclusion about the effect of molecular weight on CO_2 solubility, we turn to the literature to augment our dataset. In particular, we combine our measurements with those of Gui *et al.* [24] for monomers ethylene glycol and propylene glycol and Li *et al.* [23] for oligomers of poly(ethylene glycol) (PEG). While our measurements were taken of PPG-like polyols, which have an additional methyl group on each monomer when compared to PEG, we do not expect this difference to have a significant effect on the enthalpy of CO_2 solubility due to the distance from the methyl group in PPG and the ether linkage where CO_2 tends to associate [21].

To compare the CO_2 solubility more clearly among measurements from the

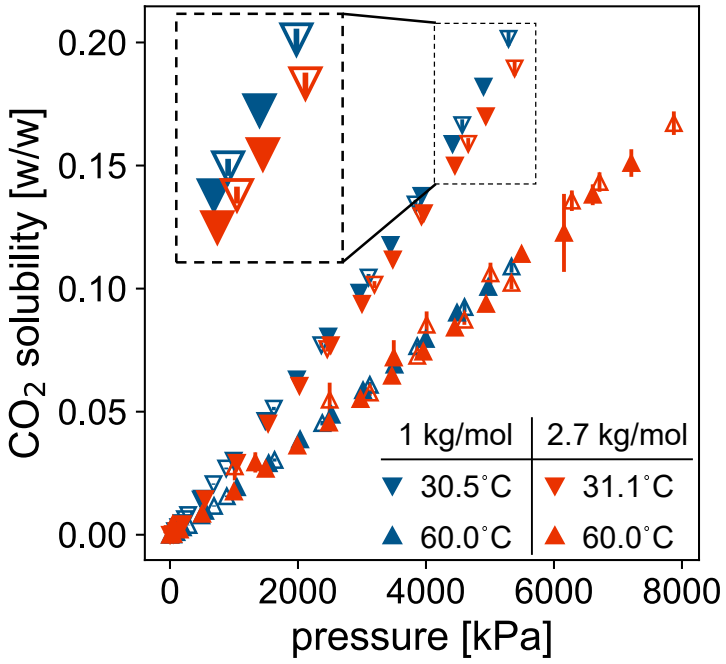

Figure II.6: The solubility of CO_2 in polyol as a function of pressure (measured with G-ADSA) is shown for difunctional polyols of two number-averaged molecular weights M_n: 1 kg/mol (blue) and 2.7 kg/mol (red). Measurements were taken during both pressurization (filled symbols) and depressurization (open symbols) of CO_2 with agreement within uncertainty. Error bars may be smaller than glyphs of some data points. Data are shown in two temperature clusters: the upper cluster contains data measured at 30.5 °C for 1000 g/mol and 31.1 °C for 2700 g/mol (downward triangles); the lower cluster contains data measured at 60 °C (upward triangles).

literature, we compared Henry's constant, the rate at which the solubility increases with pressure. We computed Henry's constant by fitting the slope of a line passing through the origin to measurements of CO_2 solubility at pressures below 1 MPa based on our observation in Figure II.5 that the solubility vs. pressure increases superlinearly at higher pressures, deviating from Henry's law. We report Henry's constant in terms of weight fraction of CO_2 per Pa [w/(w.MPa)] for comparison to other plots in this section. The only published measurements of polyether polyols that report solubility at pressures below 1 MPa were taken of difunctional polyols (two hydroxyl OH groups per chain) [23, 24]. Other measurements of CO_2 solubility available in the literature either only report solubility at pressures well above 1 MPa [5, 15, 22, 25–28] or do not report a sufficiently precise experimental uncertainty for meaningful comparison [29, 30]. Henry's constant for the CO_2 solubility in difunctional (two hydroxyl OH groups per chain) polyether polyols is shown in Figure II.7. We can see that Henry's constant increases with molecular weight

below ≈ 1000 g/mol but decreases with molecular weight above ≈ 1000 g/mol for a range of temperatures from 30 °C to 60 °C.

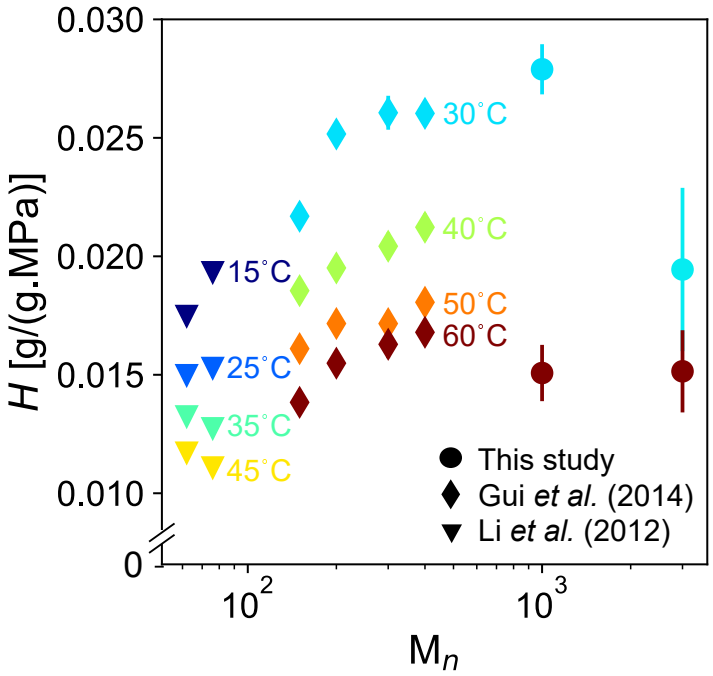

Figure II.7: Henry's constant for CO_2 solubility in difunctional polyols (two hydroxyls per chain) is plotted as a function of the average molecular weight. Both the data measured with G-ADSA in this study and literature data are provided. Error bars may be smaller than glyphs of some data points. Data are shown at different temperatures indicated by the color as defined in the legend.

Our finding of maximal CO_2 solubility in polyether polyols with a molecular weight near 1000 g/mol is consistent with the findings of Parks and Beckman for the opposite situation, the solubility of polyether polyols in CO_2 [4]. Although they made measurements at a lower temperature (25 °C) and higher pressures (tens of MPa), they also reported a maximum in the solubility of difunctional polyols at a molecular weight of 1000 g/mol. Along with other groups who have explored this question [21, 24, 31], we agree with their explanation of this non-monotonic trend based on the competition between decreasing concentration of CO_2-phobic hydroxyl groups (relative to ether linkages [21]) and decreasing mixing entropy with molecular weight. We also note that we might expect the optimal molecular weight for CO_2 solubility to decrease with temperature due to the increased importance of entropy, which favors shorter chains. Our collection of data in Figure II.7 appears to be consistent with this hypothesis at 60 °C, where the optimal molecular

weight appears to be below 1000 g/mol, but further measurements are necessary to demonstrate this behavior robustly.

II.4 Thermophysical Measurements Provide the Basis for Fitting Empirical Parameters of Thermodynamic Models

Because a single set of G-ADSA measurements (one polyol, one temperature) can last over a week, measuring the properties for all temperatures and pressures is not feasible. Instead, we turn to a thermodynamic model to estimate some of the properties (solubility, specific volume) under conditions for which we lack measurements. We chose the perturbed chain–statistical associating fluid theory (PC-SAFT) model [32] based on its success in modeling the solubility of CO_2 in polystyrene and poly(methyl methacrylate) [33]. PC-SAFT also formed a suitable basis for the development of a classical density functional theory (DFT) for modeling the interfacial tension [33], which will be discussed later in this section, as well as for an estimation of the energy barrier for bubble nucleation using the string method [34, 35], which will be discussed in Chapter VI. The application of PC-SAFT to ternary mixtures will be explored as well in Chapter VII.

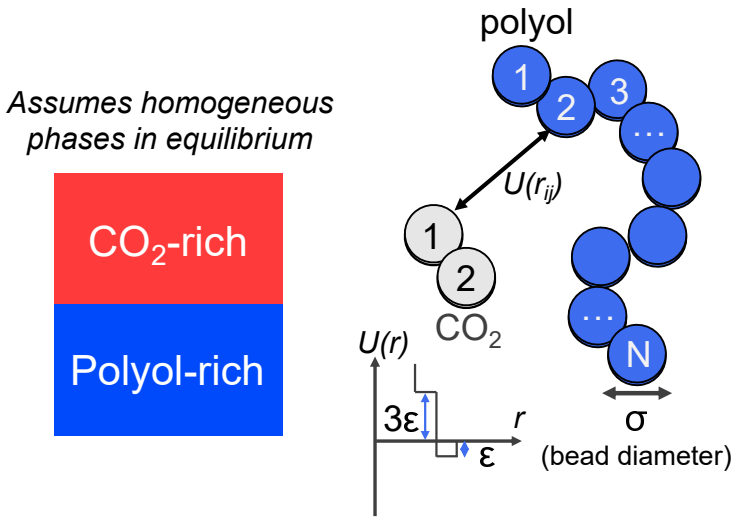

Figure II.8: A schematic of the PC-SAFT model for binary mixtures of polyol and CO_2. The model considers the polyol-rich and CO_2-rich phases as uniform and separated by an infinitesimal interface (left schematic). Both components are modeled as chains of hard-sphere beads of diameter σ (right schematic) with an attractive, radial interaction potential $U(r_{ij})$ scaled by energy parameter ε, which is plotted at the bottom of the Figure. Polyol is modeled as N beads while CO_2 is modeled as 2 beads as in [33]. Schematic adapted with permission from the unpublished work of Dr. Huikuan Chao.

The PC-SAFT model of the equation of state provides a thermodynamic model for both pure components and mixtures. It improves upon previous "SAFT" models of fluid compounds by applying a perturbation theory to a reference state of fluid of chains of purely repulsive beads, leading to the prefix "perturbed chain." A schematic of the PC-SAFT model is shown in Figure II.8. This particular application of the perturbation theory combined with the fitting of some empirical parameters to measured properties of real polymers allows PC-SAFT to model the properties of polymer mixtures better than other SAFTs (*e.g.*, PR-SAFT [33]). Due to our focus on experimental measurements, we provide only a brief, conceptual description of the PC-SAFT model sufficient to introduce the parameters to be fitted; for a detailed mathematical description of the model, see the work of Xu *et al.* [33]. The model is a mean-field theory with a free energy composed of four contributions: ideal, hard-sphere, association, and dispersion. The ideal contribution is the free energy of an ideal gas (non-interacting point particles). The hard-chain contribution is model use the Boublik–Mansoori–Carnahan–Starling–Leland (BMCSL) theory for mixtures of hard spheres with diameter σ [36, 37]. The association contribution accounts for the connectivity of the N_i beads in a chain of species i based on the bead diameter σ and density. Finally, the dispersion contribution provides an empirical model of the interactions of the molecules, which are scaled by an energy scale ε_{ij} between two species i and j. This energy scale is computed using an energy parameter ε_i for a single species i and a correction $k_{ij} = AT + B$ for fit parameters A and B and temperature T (in Kelvin) to account for differences in the interactions between two different species i and j.

Species	N (beads)	σ [Å]	ε [k_B]	k
CO_2	2	2.79	170.5	$10^{-4}(2.7T - 820)$
PPG (2700 g/mol)	123	3.01	228.5	$10^{-4}(2.7T - 820)$

Table II.2: The parameters N (number of beads per chain), σ (bead diameter in Angstroms), ε (interaction energy parameter in units of Boltzmann's constant), and k (cross-interaction parameter between the two species, unitless with T representing the temperature in Kelvin; identical for both species) that fit the solubility data for PPG (2700 g/mol) are listed. The corresponding model and experimental data are shown in Figure II.9.

Therefore, a complete PC-SAFT model of polyol and CO_2 is described by eight parameters: two chain lengths N_{CO2} and N_{polyol}, two bead diameter σ_{CO2} and σ_{polyol}, two energy parameters ε_{CO2} and ε_{polyol}, and the two parameters A and B defining the cross interaction correction term $k_{CO2,polyol} = AT + B$. Thanks to

previous work on polyol–CO_2 mixtures by Xu *et al.* [33], the parameters specific to CO_2 had already been fit to the pure-component equation of state data and were validated against NIST data [12]. The parameters for the polyol and the cross interaction were fit by Dr. Huikuan Chao through trial and error until the PC-SAFT accurately modeled the CO_2 solubility in that polyol measured with G-ADSA. Note that existing software packages that automatically fit thermodynamic model parameters are commercial, but a team from Imperial College London is extending their open-source `ypaul21/Clapeyron.jl` package [38] in `julia` for equation-of-state modeling to provide parameter estimation as well at the time of this writing [39]. As is often the case for PC-SAFT models of vapor-liquid equilibria, an infinite set of degenerate parameters for the polyol can model the CO_2 solubility. To break this degeneracy, we begin by guessing parameters based on those predicted using the group contribution method, a common method for estimating PC-SAFT parameters based on the functional groups present in the compounds [40]. These parameters result in a model that does not fit the data well, so we adjusted them manually until a fit was achieved. The PC-SAFT parameters for CO_2 and PPG (2700 g/mol) are listed in Table II.2. The CO_2 solubility predicted using these parameters is compared to the corresponding G-ADSA measurements in Figure II.9.

PC-SAFT Fits Solubility Measurements

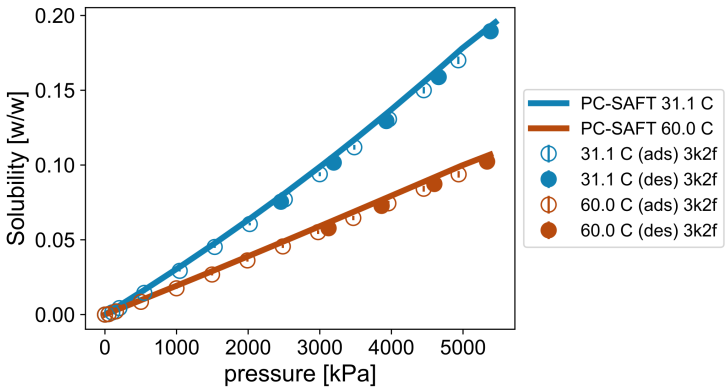

Figure II.9: CO_2 solubility in PPG of 2700 g/mol as function of pressure. Measurements from G-ADSA are shown in circular glyphs (empty indicates adsorption measurement and filled indicates desorption measurement); error bars may be smaller than the glyphs of some data points. Data were collected in the lab of Prof. Ernesto Di Maio at the University of Naples Federico II. Predicted solubility from PC-SAFT is shown in solid lines. Model was developed by Dr. Huikuan Chao in the group of Prof. Zhen-Gang Wang. Data are plotted for 31.1 °C (blue) and 60 °C (dark orange).

Because we fit the PC-SAFT parameters through trial and error, we cannot provide confidence intervals on our parameters. Instead, to demonstrate the precision of our estimate, we show the sensitivity of our predictions of different properties to ±5% variations in the σ, ε, and N parameters for PPG in Figure II.S12 of the SI. This figure shows the sensitivity of the PC-SAFT predictions of CO_2 solubility and specific volume (discussed later) and of the DFT predictions (discussed later) of interfacial tension.

DFT Model Based on PC-SAFT Models Interfacial Tension with PC-SAFT Parameters Fitted to Solubility

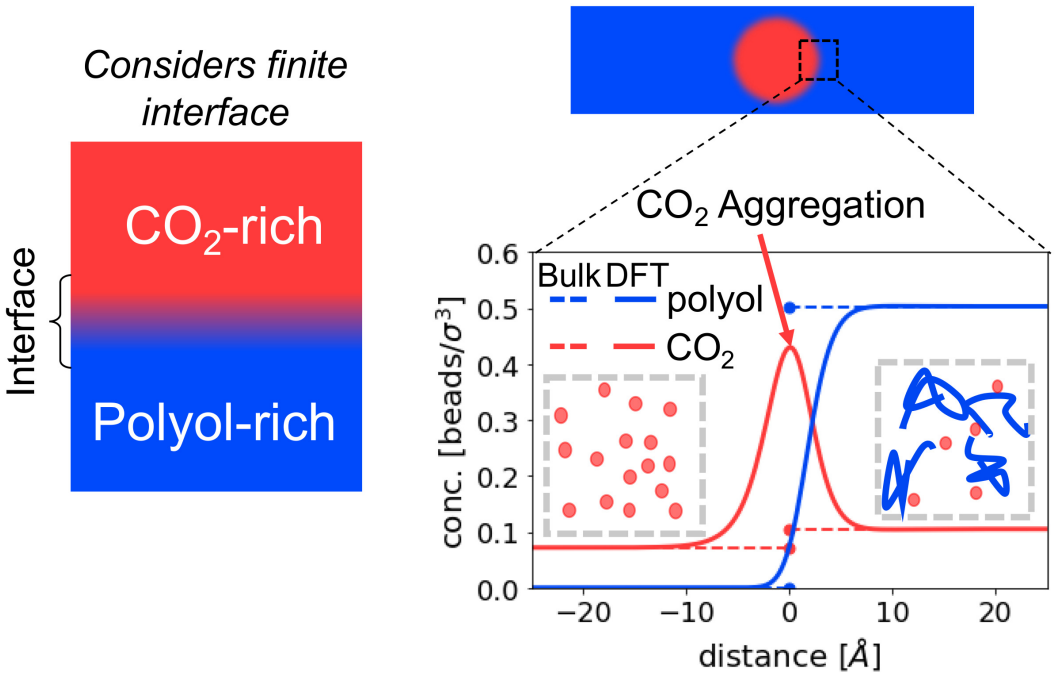

Figure II.10: Schematic of the density functional theory model of the interface between CO_2-rich and polyol-rich phases. On the left is a schematic of how DFT takes into account the non-uniformities along the finite interface. On the right is an example plot of the concentration of polyol (blue) and CO_2 (red) in the CO_2-rich phase (left), the polyol-rich phase (right), and along the interface (center) between a CO_2-rich bubble and a polyol-rich mother phase (depicted in schematic above the plot). This plot reveals an accumulation of CO_2 along the interface (indicated by red arrow; see Section II.S5 for further discussion) and other discrepancies between the DFT (solid lines) and the bulk phase concentrations predicted by PC-SAFT (dashed lines). Plot generated from the calculations of Dr. Huikuan Chao.

Based on the PC-SAFT model described above, Dr. Huikuan Chao developed a model of the interface between the polyol-rich and CO_2-rich phases with classical density functional theory (DFT) following the method described in Xu *et*

al. [33]. A schematic of the DFT model used is shown in Figure II.10. The result is a model that takes the PC-SAFT parameters fitted to experimental CO_2 solubility data as input and predicts the equilibrium concentration profile of each species and the resulting interfacial tension at an interface between two phases. An example of the equilibrium concentration profile of CO_2 and PPG is shown in Figure II.S14 of the SI; here, we will focus on the predicted interfacial tension. This value is not fitted in any way to the values of interfacial tension measured with G-ADSA; therefore, we can test the validity of this model by comparing its blind prediction to the experimental data, following the method described by Xu *et al.* [33]. The prediction of the interfacial tension between the CO_2-rich and polyol-rich phases of a mixture of CO_2 and PPG (2700 g/mol) is shown in Figure II.11. We see that the DFT model not only predicts the qualitative trends observed in the experimental measurements, such as decreasing interfacial tension with temperature at low pressure and increasing interfacial tension with temperature at high pressure, but also achieves reasonable, though not perfect, quantitative accuracy. This agreement between model and measurement supports our use of the DFT model for predictions of interfacial properties and provides our justification for using this model as the basis of our string method predictions of the energy barrier for bubble nucleation discussed in Chapter VI.

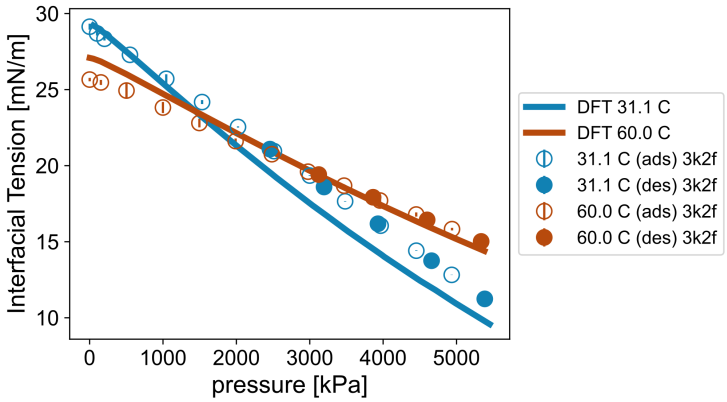

Figure II.11: Interfacial tension between polyol-rich and CO_2-rich phases of a mixture of CO_2 and PPG (2700 g/mol) predicted by DFT model based on parameters from fitting PC-SAFT model to solubility data (see Fig. II.9) shown in solid lines compared to measurements from G-ADSA shown in circular glyphs (empty indicates adsorption measurement and filled indicates desorption measurement). Error bars may be smaller than the glyphs of some data points. Data are plotted for 31.1 °C (blue) and 60 °C (dark orange). Data were collected in the lab of Prof. Ernesto Di Maio at the University of Naples Federico II. Model was developed by Dr. Huikuan Chao in the group of Prof. Zhen-Gang Wang.

PC-SAFT Fails to Model Specific Volume

Despite the success of PC-SAFT in modeling CO_2 solubility and DFT in modeling interfacial tension for polyol–CO_2 mixtures, it fails to model the specific volume. While there is an infinite set of degenerate PC-SAFT parameters for which the PC-SAFT model accurately describes the measured CO_2 solubility and the DFT model accurately describes the measured interfacial tension, no group of parameters in that set yields an accurate PC-SAFT model of the specific volume. The disagreement between the specific volume measured with G-ADSA and the predictions of PC-SAFT model based on the parameters in Table II.2 is shown in Figure II.12. Qualitatively, while the PC-SAFT model accurately captures the effect of temperature and high pressure on specific volume, it fails to capture the non-monotonic dependence of the specific volume on pressure at low pressures and temperatures. This failure of PC-SAFT's coarse-grained beads to capture this behavior is not surprising given that it arises due to the molecular structure [18–20]. Quantitatively, however, PC-SAFT underestimates the specific volume (overestimates the density) by over 10%. For the sake of providing model predictions to compare to experimental measurements, we accept the failure of our PC-SAFT model to predict the specific volume accurately and ignore the association of the hydroxyl end groups.

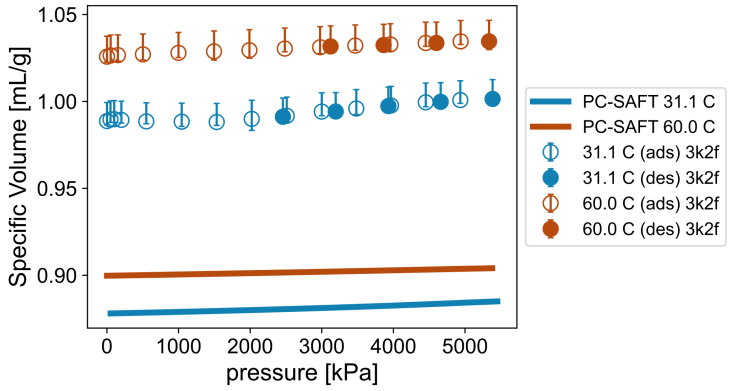

Figure II.12: The specific volume of a mixture of CO_2 and PPG (2700 g/mol) as a function of pressure predicted by PC-SAFT (solid lines) and measured with G-ADSA (circular glyphs: empty indicates adsorption measurement and filled indicates desorption measurement). Error bars may be smaller than the glyphs of some data points. Data are plotted for 31.1 °C (blue) and 60 °C (dark orange). Upper error bars indicate systematic error and lower error bars indicate statistical error. Data are shown at 31 °C (blue) and 60 °C (red). Data were collected in the lab of Prof. Ernesto Di Maio at the University of Naples Federico II. Model was developed by Dr. Huikuan Chao in the group of Prof. Zhen-Gang Wang.

II.5 Recommendation for Future Work

Based on the conclusion of Parks and Beckman that "a complete description of the phase behavior of these CO_2–polyol mixtures may require a more rigorous model of hydrogen bonding" [4], we are hopeful that the proper incorporation of the association of the hydroxyl end groups of the polyol can yield an accurate model for both CO_2 solubility and specific volume. The incorporation of the association of the end groups was explored with some success by Dr. Huikuan Chao, but the extension of such a model to DFT and, ultimately, to the string method would be a colossal task.

References

1. Pastore Carbone, M. G., Di Maio, E., Iannace, S. & Mensitieri, G. Simultaneous experimental evaluation of solubility, diffusivity, interfacial tension and specific volume of polymer/gas solutions. *Polymer Testing* **30,** 303–309. ISSN: 01429418. https://linkinghub.elsevier.com/retrieve/pii/S0142941811000067 (May 2011).

2. Di Caprio, M. R. *et al.* Polyether polyol/CO2 solutions: Solubility, mutual diffusivity, specific volume and interfacial tension by coupled gravimetry-Axisymmetric Drop Shape Analysis. *Fluid Phase Equilibria* **425,** 342–350. ISSN: 03783812. https://linkinghub.elsevier.com/retrieve/pii/S0378381216302990 (Oct. 2016).

3. Di Caprio, M. R. *et al. Thermosetting polyurethane foams by supercritical CO 2 as physical blowing agent* tech. rep. (University of Naples Federico II, Naples, 2017).

4. Parks, K. L. & Beckman, E. J. Generation of microcellular polyurethane foams via polymerization in carbon dioxide. I: Phase behavior of polyurethane precursors. *Polymer Engineering & Science* **36,** 2404–2416. ISSN: 0032-3888. https://onlinelibrary.wiley.com/doi/10.1002/pen.10639 (Oct. 1996).

5. Yang, Z. *et al.* Effect of the properties of polyether polyol on sorption behaviour and interfacial tension of polyol/CO2 solutions under high pressure condition. *The Journal of Chemical Thermodynamics* **133,** 29–36. ISSN: 00219614. https://linkinghub.elsevier.com/retrieve/pii/S0021961419300643 (June 2019).

6. Kluyver, T. *et al.* in *Positioning and Power in Academic Publishing: Players, Agents and Agendas* (eds Loizides, F. & Schmidt, B.) 87–90 (IOS Press, 2016). ISBN: 9781614996484. https://ebooks.iospress.nl/ISBN/978-1-61499-648-4.

7. Hunter, J. D. Matplotlib: A 2D Graphics Environment. *Computing in Science & Engineering* **9,** 90–95. ISSN: 1521-9615. http://ieeexplore.ieee.org/document/4160265/ (2007).

8. Harris, C. R. *et al.* Array programming with NumPy. *Nature* **585,** 357–362. ISSN: 0028-0836. arXiv: 2006.10256. https://www.nature.com/articles/s41586-020-2649-2 (Sept. 2020).

9. Reback, J. *et al. pandas-dev/pandas: Pandas 1.0.1* 2022. 10.5281/zenodo.5893288.

10. Virtanen, P. *et al.* SciPy 1.0: fundamental algorithms for scientific computing in Python. *Nature Methods* **17,** 261–272. ISSN: 1548-7091. arXiv: 1907.10121. http://www.nature.com/articles/s41592-019-0686-2 (Mar. 2020).

11. Ylitalo, A. S. *andylitalo/g-adsa: v0.1.0* 2022. https://github.com/andylitalo/g-adsa (2022).

12. NIST. *NIST Standard Reference Database Number 69* 2022. https://webbook.nist.gov/chemistry/ (2022).

13. Crank, J. *The Mathematics of Diffusion* 2nd Ed., 1–352 (Oxford University Press, London, 1975).

14. Song, B. & Springer, J. Determination of interfacial tension from the profile of a pendant drop using computer-aided image processing. *Journal of Colloid and Interface Science* **184,** 64–76. ISSN: 00219797 (1996).

15. Guadagno, T. & Kazarian, S. G. High-Pressure CO 2 -Expanded Solvents: Simultaneous Measurement of CO 2 Sorption and Swelling of Liquid Polymers with in-Situ Near-IR Spectroscopy. *The Journal of Physical Chemistry B* **108,** 13995–13999. ISSN: 1520-6106. https://pubs.acs.org/doi/abs/10.1021/jp0481097%20https://pubs.acs.org/doi/10.1021/jp0481097 (Sept. 2004).

16. Rajendran, A. *et al.* Simultaneous measurement of swelling and sorption in a supercritical CO2-poly(methyl methacrylate) system. *Industrial and Engineering Chemistry Research* **44,** 2549–2560. ISSN: 08885885 (Apr. 2005).

17. Carbone, M. G. P., Di Maio, E., Scherillo, G., Mensitieri, G. & Iannace, S. Solubility, mutual diffusivity, specific volume and interfacial tension of molten PCL/CO2 solutions by a fully experimental procedure: effect of pressure and temperature. *The Journal of Supercritical Fluids* **67,** 131–138. http://dx.doi.org/10.1016/j.supflu.2012.04.001 (2012).

18. Pastore Carbone, M. G., Di Maio, E., Musto, P., Braeuer, A. & Mensitieri, G. On the unexpected non-monotonic profile of specific volume observed in PCL/CO2 solutions. *Polymer* **56,** 252–255. ISSN: 00323861. https://linkinghub.elsevier.com/retrieve/pii/S0032386114010568 (Jan. 2015).

19. Carbone, M. G. P. *et al.* Raman Line Imaging of Poly(e-caprolactone)/Carbon Dioxide Solutions at High Pressures: A Combined Experimental and Computational Study for Interpreting Intermolecular Interactions and Free-Volume Effects. *Journal of Physical Chemistry B* **120,** 9115–9131. ISSN: 15205207. https://pubs.acs.org/sharingguidelines (Sept. 2016).

20. Mensitieri, G., Scherillo, G., Panayiotou, C. & Musto, P. Towards a predictive thermodynamic description of sorption processes in polymers: The synergy between theoretical EoS models and vibrational spectroscopy. *Materials Science and Engineering: R: Reports* **140,** 100525. ISSN: 0927796X. https://linkinghub.elsevier.com/retrieve/pii/S0927796X19301275 (Apr. 2020).

21. Kilic, S. *et al. Phase behavior of oxygen-containing polymers in CO2* in *Macromolecules* **40** (American Chemical Society, Feb. 2007), 1332–1341. https://pubs.acs.org/sharingguidelines.

22. Daneshvar, M., Kim, S. & Gulari, E. High-pressure phase equilibria of polyethylene glycol-carbon dioxide systems. *The Journal of Physical Chemistry* **94,** 2124–2128. ISSN: 0022-3654. https://pubs.acs.org/doi/10.1021/j100368a071 (Mar. 1990).

23. Li, J., Ye, Y., Chen, L. & Qi, Z. Solubilities of CO 2 in poly(ethylene glycols) from (303.15 to 333.15) K. *Journal of Chemical and Engineering Data* **57,** 610–616. ISSN: 00219568. https://pubs.acs.org/sharingguidelines (Feb. 2012).

24. Gui, X., Tang, Z. & Fei, W. Solubility of CO2 in alcohols, glycols, ethers, and ketones at high pressures from (288.15 to 318.15) K. *Journal of Chemical and Engineering Data* **56,** 2420–2429. ISSN: 00219568. https://pubs.acs.org/sharingguidelines (May 2011).

25. Weidner, E., Wiesmet, V., Knez, Ž. & Škerget, M. Phase equilibrium (solid-liquid-gas) in polyethyleneglycol-carbon dioxide systems. *The Journal of Supercritical Fluids* **10,** 139–147. ISSN: 08968446. https://linkinghub.elsevier.com/retrieve/pii/S0896844697000168 (Aug. 1997).

26. Aionicesei, E., Škerget, M. & Knez, Ž. Measurement and modeling of the CO2 solubility in polyethylene glycol of different molecular weights. *Journal of Chemical and Engineering Data* **53,** 185–188. ISSN: 00219568. https://pubs.acs.org/sharingguidelines (Jan. 2008).

27. Medina-Gonzalez, Y. *et al.* Phase equilibrium of the CO2/glycerol system: Experimental data by in situ FT-IR spectroscopy and thermodynamic modeling. *The Journal of Supercritical Fluids* **73,** 97–107. https://hal.archives-ouvertes.fr/hal-00877680/document (2013).

28. Nunes, A. V., Carrera, G. V., Najdanovic-Visak, V. & Nunes da Ponte, M. Solubility of CO2 in glycerol at high pressures. *Fluid Phase Equilibria* **358,**

105–107. ISSN: 0378-3812. https://www.sciencedirect.com/science/article/pii/S0378381213004172 (Nov. 2013).

29. Aschenbrenner, O. & Styring, P. Comparative study of solvent properties for carbon dioxide absorption. *Energy Environ. Sci.* **3,** 1106–1113. www.rsc.org/ees (2010).

30. Wiesmet, V., Weidner, E., Behme, S., Sadowski, G. & Arlt, W. Measurement and modelling of high-pressure phase equilibria in the systems polyethyleneglycol (PEG)–propane, PEG–nitrogen and PEG–carbon dioxide. *The Journal of Supercritical Fluids* **17,** 1–12. ISSN: 08968446 (Feb. 2000).

31. Girard, E., Tassaing, T., Marty, J.-D. & Destarac, M. Structure–Property Relationships in CO 2 -philic (Co)polymers: Phase Behavior, Self-Assembly, and Stabilization of Water/CO 2 Emulsions. *Chemical Reviews* **116,** 4125–4169. ISSN: 0009-2665. https://pubs.acs.org/doi/10.1021/acs.chemrev.5b00420 (Apr. 2016).

32. Gross, J. & Sadowski, G. Perturbed-Chain SAFT: An Equation of State Based on a Perturbation Theory for Chain Molecules. *Ind. Eng. Chem. Res.* **40,** 1244–1260. https://pubs.acs.org/doi/abs/10.1021/ie0003887 (2001).

33. Xu, X., Cristancho, D. E., Costeux, S. & Wang, Z.-G. Density-functional theory for polymer-carbon dioxide mixtures: A perturbed-chain SAFT approach. *The Journal of Chemical Physics* **137,** 054902. ISSN: 0021-9606. http://aip.scitation.org/doi/10.1063/1.4742346 (Aug. 2012).

34. Xu, X., Cristancho, D. E., Costeux, S. & Wang, Z.-G. Discontinuous Bubble Nucleation Due to a Metastable Condensation Transition in Polymer–CO2 Mixtures. *The Journal of Physical Chemistry Letters* **4,** 1639–1643. http://pubs.acs.org/doi/10.1021/jz4005575 (May 2013).

35. Xu, X., Cristancho, D. E., Costeux, S. & Wang, Z.-G. Bubble nucleation in polymer–CO2 mixtures. *Soft Matter* **9,** 9675. ISSN: 1744-683X. www.rsc.org/softmatter%20http://xlink.rsc.org/?DOI=c3sm51477c (2013).

36. Boublík, T. Hard - Sphere Equation of State. *The Journal of Chemical Physics* **53,** 471–472. ISSN: 0021-9606. http://aip.scitation.org/doi/10.1063/1.1673824 (July 1970).

37. Mansoori, G. A., Carnahan, N. F., Starling, K. E. & Leland, T. W. Equilibrium thermodynamic properties of the mixture of hard spheres. *The Journal of Chemical Physics* **54,** 1523–1526. ISSN: 00219606 (1971).

38. Riedemann, A. *et al. ypaul21/Clapeyron.jl: v0.3.5* 2022. https://github.com/ypaul21/Clapeyron.jl.

39. Walker, P. J., Yew, H.-W. & Riedemann, A. Clapeyron.jl: An extensible, open-source fluid-thermodynamics toolkit, 1–67. arXiv: 2201.08927. http://arxiv.org/abs/2201.08927 (2022).

40. Tihic, A., Kontogeorgis, G. M., von Solms, N., Michelsen, M. L. & Constantinou, L. A Predictive Group-Contribution Simplified PC-SAFT Equation of State: Application to Polymer Systems. *Industrial & Engineering Chemistry Research* **47,** 5092–5101. ISSN: 0888-5885. https://pubs.acs.org/doi/10.1021/ie0710768 (Aug. 2008).

II.S1 Gravimetry–Axisymmetric Drop Shape Analysis (G-ADSA)

Apparatus

As described in Section II.1, the Teflon rod swelled as a result of absorbing CO_2 as the pressure increased. This swelling is depicted in Figure II.S1. An image of the interior of the G-ADSA apparatus is shown in panel (a) as well for reference, with the Teflon rod marked by a box.

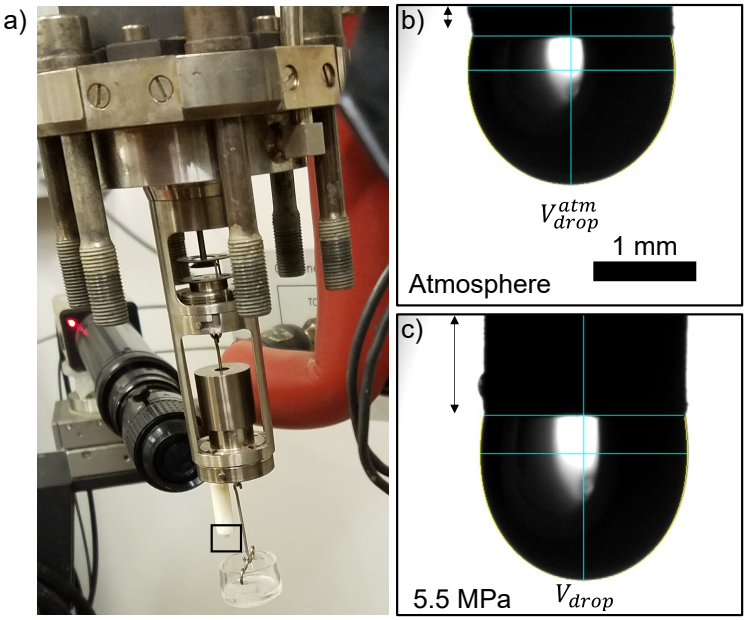

Figure II.S1: Swelling of Teflon rod for suspending pendant drop in G-ADSA due to absorption of CO_2. a) Interior of G-ADSA setup with tip of Teflon rod outlined in a black square. Images of the Teflon rod are recorded with the camera seen behind the rod. b) Image of Teflon rod under atmospheric pressure. c) Image of Teflon rod camera under 5.5 MPa of CO_2. Note that the tip of the Teflon rod has descended due to the swelling of the rod from absorption of CO_2.

Data Analysis

Having briefly described the methods for estimating CO_2 solubility, specific volume, interfacial tension, and CO_2 diffusivity for polyol–CO_2 mixtures using G-ADSA measurements, we now describe the analysis in greater depth and mathematical detail below. This analysis is encoded in the GitHub repository `andylitalo/g-adsa` [1].

We begin by estimating the equilibrium volume of the pendant drop from the image of the drop shape using the commercial software FTA32 developed by First Ten Angstroms. The software only requires that we click the leftmost and rightmost points of contact between the pendant drop and the Teflon rod and provide a length

scale for the pixels in the image. To determine the length scale, we divide the known width of the tip of the rod (measured with calipers) by its width in pixels in the image taken under vacuum—at higher pressures, the Teflon rod swells. Finally, the software estimates the equilibrium drop volume V_{drop} by assuming axisymmetry. We assume that the equilibrium drop volume $V_{drop}(p)$ grows with pressure p in proportion to the equilibrium sample volume $V_{samp}(p)$,

$$V_{samp}(p) = \frac{V_{drop}(p)}{V_{drop}(0)} V_{samp}(0) \tag{II.1}$$

Next, we estimate the equilibrium sample mass. In this Section, we will use the letter B to indicate a direct measurement of force by the Rubotherm balance in the G-ADSA apparatus (scaled by the gravitational acceleration g to be in units of mass), m to indicate mass, $\tilde{m}$ to indicate a force on the balance (buoyancy) scaled to be in units of mass, and w to indicate a mass fraction (kg/kg). The balance provides us readings of the apparent weight $B_{app}(p)$ and the tare weight $B_{tare}(p)$ at the given pressure. Because these weights are scaled by the gravitational acceleration, they correspond to the mass of the components of the scale minus the buoyant force from the surrounding atmosphere. Thus, the difference between these measurements $\Delta B(p) \equiv B_{app}(p) - B_{tare}(p)$ is equivalent to the sum of the mass of the sample at the equilibrium pressure $m_{samp}(p)$, the mass of the crucible m_{cruc}, and the mass of the hooks m_{hook} minus the buoyant force scaled by gravitational acceleration $\tilde{m}_{buoy}(p)$ at the equilibrium pressure (note that the buoyant force must be accounted for due to the precision of these measurements),

$$\Delta B(p) = m_{samp}(p) + m_{cruc} + m_{hook} - \tilde{m}_{buoy}(p) \tag{II.2}$$

When the pressure $p = 0$, the mass of the sample is the dry mass of the polyol $m_{samp}(p = 0) \equiv m_{poly}$ (assumed to be constant, *i.e.* negligible vaporization of polyol) and there is no buoyant force ($\tilde{m}_{buoy}(p = 0) = 0$). Thus, the difference in balance readings at zero pressure is

$$\Delta B(p = 0) = m_{poly} + m_{cruc} + m_{hook} \tag{II.3}$$

Subtracting equation II.3 from equation II.2 gives

$$\Delta B(p) - \Delta B(p = 0) = m_{samp} - m_{poly} - m_{buoy}(p)$$

The sample mass m_{samp} is composed of the mass of the dry polyol m_{poly} and the mass of the gas m_{gas}, such that the equation above can be solved for the mass of the gas,

$$m_{gas}(p) = \Delta B(p) - \Delta B(p = 0) + m_{buoy}(p) \tag{II.4}$$

We now only require the effect of the buoyant force on the balance reading $\tilde{m}_{buoy}(p)$ to compute the mass of dissolved gas. When scaled by gravitational acceleration, the buoyant force on the balance reading is the density of the CO_2 atmosphere at the given pressure and temperature T, $\rho_{CO2}(p, T)$ (available on the NIST Chemistry WebBook[2]), multiplied by the total volume of weighed objects V_{tot}. The total volume of weighed objects includes the volumes of the crucible V_{cruc}, the supporting hooks V_{hook}, and the sample $V_{samp}(p)$. Thus, the buoyant force is

$$\tilde{m}_{buoy}(p) = \rho_{CO2}(p)[V_{cruc} + V_{hook} + V_{samp}(p)] \tag{II.5}$$

The volume of the crucible and hooks V_{cruc}+V_{hook} was measured to be 2.2675 mL by Dr. Maria Rosaria Di Caprio in a helium atmosphere before performing experiments, as described in previous work [3]. The volume of the sample at the given pressure $V_{samp}(p)$ can be calculated with equation II.1.

The mass of dissolved gas can thus be computed by plugging the result of equation II.5 into equation II.4. To compute the solubility of CO_2 in the polyol, we also need the dry mass polyol, m_{poly}. While we measured the polyol mass in the atmosphere beforehand, we expect that the polyol had absorbed some of the moisture from the humid, Neapolitan summertime atmosphere. We therefore solve equation II.3 for m_{poly}

$$m_{poly} = \Delta B(p = 0) - (m_{cruc} + m_{hook}) \tag{II.6}$$

and plug in the known difference in balance readings at zero pressure $\Delta B(p = 0)$ and mass of the crucible and supporting hooks $m_{cruc} + m_{hook}$ to compute the dry

polyol mass. Having computed the gas mass at the given pressure $m_{gas}(p)$ and dry polyol mass m_{poly}, we compute the solubility by mass of CO_2 in the polyol,

$$w_{CO2}(p) = \frac{m_{gas}(p)}{m_{gas}(p) + m_{poly}} \tag{II.7}$$

Next, we compute the specific volume of the sample, which is the sample volume $V_{samp}(p)$ divided by the sample mass $m_{samp}(p)$. Noting that the sum of the gas mass and dry polyol mass gives the sample mass $m_{samp}(p) = m_{gas}(p) + m_{poly}$, the specific volume is

$$v(p) = \frac{V_{samp}(p)}{m_{samp}(p)} \tag{II.8}$$

To estimate the diffusivity, we followed the model derived by Crank for diffusion into a slab [4]. The model considers an infinite slab of fluid with a concentration dependent diffusivity with thickness $2l$ and a gas atmosphere on both sides, as shown in Figure II.S2. In our case, the polyol sample is only open to the CO_2 atmosphere on one side. The situation is nevertheless analogous if we map the midpoint of the slab ($x = 0$) to the base of the crucible because there is no flux through either surface. We can therefore treat the top half of the slab in the model as our sample in the crucible, where the parameter $l = h_{samp}$, the height of our sample.

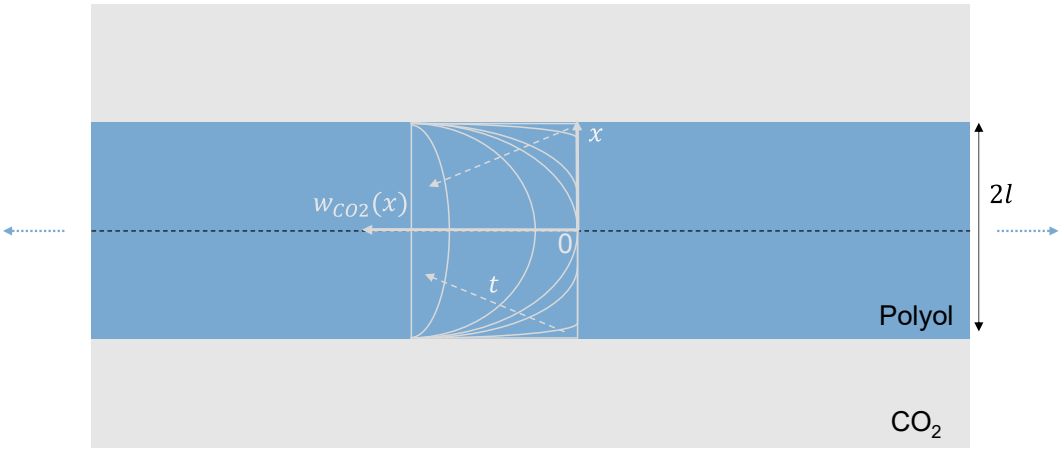

Figure II.S2: Schematic of diffusion of CO_2 (gray) into a slab of polyol (blue) with width l and infinite horizontal extent.

With this model, we can estimate the diffusivity of CO_2 as a function of the saturation pressure $\mathcal{D}(p)$ in the sample in two ways: (1) fit a square-root function to the mass of dissolved gas over time $m_{gas}(t)$ at early times and (2) fit an

exponential function to the mass of dissolved gas over time $m_{gas}(t)$ upon approaching equilibrium. While we used both to estimate the diffusivity, we generally used the first method (square root) due to better fitting of the data and lower sensitivity to noise. We begin by deriving the diffusivity from an early-time square-root fit. In the book *The Mathematics of Diffusion*, Crank derives the mass of dissolved gas over time at short times (see equation 4.20 on p. 48 of [4]). We adapt the notation of the equation below, where $m(t)$ corresponds to $m_{gas}(t)$, its value at infinity $m(t \to \infty)$ is the equilibrium value of the mass of dissolved gas, $m_{gas}(p)$, the diffusivity D is the diffusivity of CO_2 at the equilibrium pressure $\mathcal{D}(p)$, and the size parameter corresponds to the height of our sample $l = h_{samp}$, as mentioned earlier,

$$\frac{m_{gas}(t)}{m_{gas}(p)} = 2\left(\frac{\mathcal{D}(p)t}{h_{samp}^2}\right)^{1/2}\left\{\pi^{-1/2} + 2\sum_{n=1}^{\infty}(-1)^n \,\mathrm{ierfc}\left(\frac{nh_{samp}}{\sqrt{\mathcal{D}(p)t}}\right)\right\} \tag{II.9}$$

where ierfc is the integral of the complementary error function and $\mathcal{D}$ is an average diffusivity in the material. Due to the complexity of deriving an accurate formula to average the diffusivity within the sample, we will keep the changes in pressure between measurements small enough so the diffusivity throughout the sample will be close to the diffusivity at equilibrium for the given pressure $\mathcal{D}(p)$. The results of this assumption are seen in Figure II.4, where the estimated diffusivity is larger during depressurization $\mathcal{D}_{dp}(p)$, when the diffusivity in the sample starts higher than the equilibrium value, than during pressurization $\mathcal{D}_p(p)$, when diffusivity in the sample starts lower than the equilibrium, *i.e.* $\mathcal{D}_p(p) < \mathcal{D}(p) < \mathcal{D}_{dp}(p)$. The errors incurred by applying large changes in pressure, especially during depressurization, can also be seen.

At short times $t \ll \frac{l^2}{\mathcal{D}}$, the terms in the summation are negligible, and we can simplify this equation to

$$\frac{m_{gas}(t)}{m_{gas}(p)} = \frac{2}{\sqrt{\pi}}\left(\frac{\mathcal{D}t}{l^2}\right)^{1/2} \tag{II.10}$$

If we assume that the swelling of the sample is negligible at short times, then the initial gradient of the mass of dissolved gas with respect to the square root of time $\frac{\mathrm{d}}{\mathrm{d}\sqrt{t}}\left(\frac{m_{gas}(t)}{m_{gas}(p)}\right)\Big|_{t=t_0} = \frac{2}{\sqrt{\pi}}\left(\frac{\mathcal{D}}{l^2}\right)^{1/2}$, where t_0 is the time at which the concentration of gas in the surrounding atmosphere is changed. Thus, the diffusivity of CO_2 at pressure p is

$$\mathcal{D}(p) = \frac{\pi h_{samp}^2}{4}\left[\frac{\mathrm{d}}{\mathrm{d}\sqrt{t}}\left(\frac{m_{gas}(t)}{m_{gas}(p)}\right)\bigg|_{t=t_0}\right]^2 \tag{II.11}$$

Knowing that the mass of dissolved gas $m_{gas}(t)$ will grow as $t^{1/2}$ from equation II.10, we fit the measurement of dissolved gas over time, $m_{gas}(t)$, which can be calculated by noting that $m_{gas}(t)$ is $m_{gas}(p)$ computed at a moment in time rather than at the equilibrium pressure. Thus, we can compute $m_{gas}(t)$ using equation II.4 where measurements taken at the equilibrium pressure p are replaced measurements at a particular time t,

$$m_{gas}(t) = \Delta B(t) - \Delta B(p = 0) + \tilde{m}_{buoy}(t) \tag{II.12}$$

We fit $m_{gas}(t)$ to the function

$$m_{gas}(t) = a\sqrt{t - t_0} + m_{gas}(p_{prev}) \tag{II.13}$$

for positive real constants a, t_0, where $m_{gas}(p_{prev})$ is the mass of gas measured at the previous equilibrium pressure. We compared the quality of fit to the data of this function to three other fit functions: (1) equation II.13 where t_0 was specified as the time when the pressure was changed, (2) equation II.13 where t_0 was specified as in (1) but $m_{gas}(p_{prev})$ was a fitted parameter, and (3) equation II.13 where both t_0 and $m_{gas}(p_{prev})$ were fitted parameters. The form shown in equation II.13 yielded the best fits to the data, so we used it for fitting. An example fit to the transient sample mass is shown in Figure II.S3.

By fitting $m_{gas}(t)$ to a square-root growth in time, we find that the derivative we must compute in equation II.11 is $\frac{\mathrm{d}}{\mathrm{d}\sqrt{t}} m_{gas}(t) = a$, one of the fitting parameters in equation II.13. Therefore, our estimation for the diffusivity at a given pressure based on a square-root fit is

$$\mathcal{D}(p) = \frac{\pi h_{samp}^2}{4}\left(\frac{a}{m_{gas}(p)}\right)^2 \tag{II.14}$$

In some cases, we also use the exponential-fit method to estimate the diffusivity, such as when comparing to an estimate based on an exponential fit in the literature in Figure II.S10. Below, we describe the derivation of this estimation

method. This estimation method considers the latest stages of diffusion as the system approaches equilibrium. Crank demonstrates that the mass of a sample in an atmosphere of diffusing gas obeys the following equation (equation 10.168) [4],

$$\frac{\mathrm{d}}{\mathrm{d}t}\left[\log(m(t) - m(t \to \infty)\right] = -\frac{\mathcal{D}\pi^2}{4h_{samp}^2} \tag{II.15}$$

where we have substituted $2h_{samp}$ for the length scale l, which is the full width of the slab (rather than half the width) in this section of Crank's book. At late enough times, the concentration is close enough to the equilibrium value that the effect of the changing concentration in the system on the diffusion coefficient $\mathcal{D}(p)$ is negligible. Therefore, in this model, we assume that $\mathcal{D}(p)$ is constant and corresponds to the diffusion coefficient at the equilibrium concentration.

We then integrate equation II.15 to arrive at the following functional form for the mass of the sample,

$$m(t) - m(t \to \infty) = [m(t=0) - m(t \to \infty)] \exp\left[-\frac{\mathcal{D}\pi^2}{4h_{samp}^2}t\right]$$

$$\frac{m(t \to \infty) - m(t)}{m(t \to \infty) - m(t=0)} = \exp\left[-\frac{\mathcal{D}\pi^2}{4h_{samp}^2}t\right]$$

Note that, as opposed to the case for the $t^{1/2}$ fit, $m(t=0)$ is the mass of the sample at the beginning of the exponential behavior (which we define as $t = 0$). We can then perform a fit of the mass of absorbed gas to the following functional form,

$$m(t) = A \exp\left[Bt\right] + C$$

where A, B, and C are fitting parameters. An example fit to the transient sample mass is shown in Figure II.S3. Then C is the equilibrium mass of absorbed gas $m(t \to \infty)$ and B can be related to the diffusion constant $\mathcal{D}$ by the following equation,

$$\mathcal{D} = -\frac{4h_{samp}^2}{\pi^2} B \tag{II.16}$$

giving the exponential-fit estimate of the diffusivity $\mathcal{D}$. Note that the change in h_{samp} during the course of a pressure step is negligible relative to the error in the fitted parameter B (at most 2%).

In practice, we only measure a range for $\mathcal{D}(p)$, with the measurement taken upon pressurization $\mathcal{D}_p(p)$ providing the lower bound and the measurement taken upon depressurization $\mathcal{D}_{dp}(p)$ providing the upper bound.

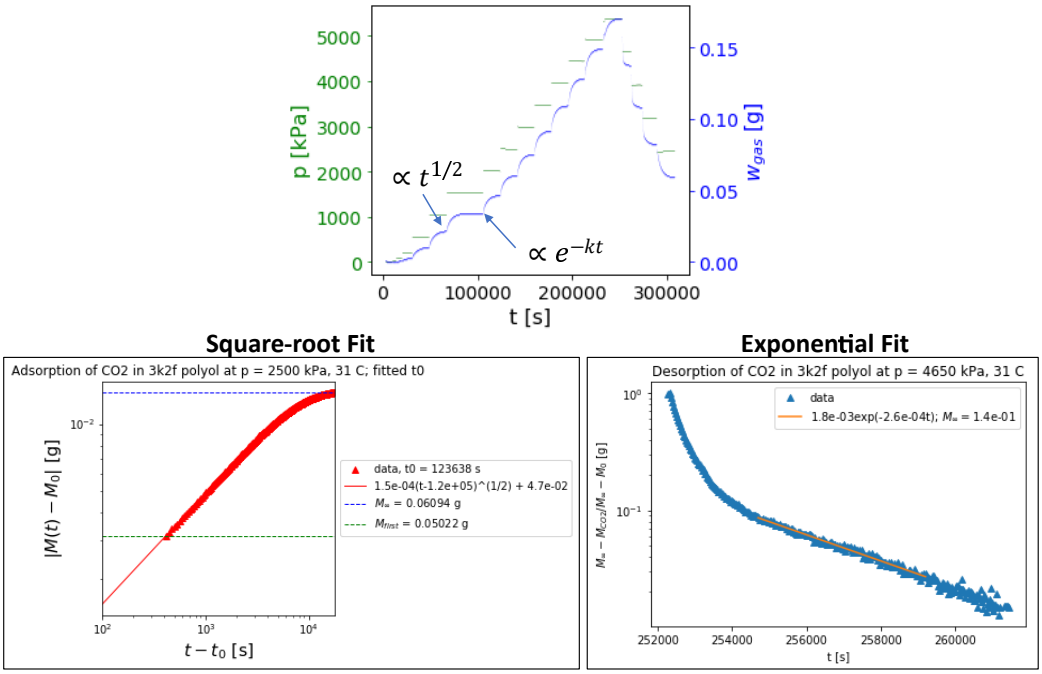

Figure II.S3: Plots of the transient mass absorption and desorption from the polyol–CO_2 sample over time. Polyol is PPG 2700 g/mol measured at 31.1 °C. Top: pressure (green, left vertical axis) and dissolved weight fraction of CO_2 (w_{gas}, blue, right vertical axis) as a function of time for a full G-ADSA experiment. Note that the initial transient of the weight fraction goes as the square root of time while the end of the transient nearing equilibrium goes as exponential decay. Lower left: an example fit of square-root function to the initial transient dissolved mass of CO_2 measured relative to the initial mass upon changing the pressure. Lower right: an example fit of exponential decay to the final transient dissolved mass of CO_2 measured relative to the estimated equilibrium mass. Fit parameters shown in legend.

Finally, we estimate the interfacial tension at a given pressure $\gamma(p)$ using axisymmetric drop shape analysis (ADSA) performed with the commercial software First Ten Angstroms 32 (FTA32). This software automatically detects the edge

of the drop and fits a contour consistent with the predictions for a pendant drop to the detected edge. When provided the density of the drop (reciprocal of the specific volume $1/v(p)$) and the density of the CO_2-rich atmosphere (estimated using the p-v-T data for pure CO_2 available from NIST[2]), the software computes the interfacial tension. To learn more about the pendant drop method and its estimation of interfacial tension, see the work of Song and Springer [5]. Because ADSA was performed using a camera separate from the Rubotherm MSB used for gravimetry, the two sets of measurements were synchronized to a common start time, thereby providing simultaneous measurements of each parameter.

Propagating Uncertainty in G-ADSA Measurements

To estimate the error bars shown in the plots of G-ADSA measurements, we propagated the uncertainty from all known sources of error through the analysis equations. These formulas are encoded in the `errprop.py` library of functions within the `andylitalo/g-adsa` GitHub repository [1].

Reproducibility of Results

In addition to being precise, measurements with G-ADSA are reproducible. We demonstrate their reproducibility in two ways. First, we show that the measurements made while pressurizing the system are generally statistically indistinguishable from those made while depressurizing the system—which may take place days later—with few exceptions. Second, we show that measurements from two separate experiments run under the same conditions are also generally statistically indistinguishable. We demonstrate this reproducibility using PPG (2700 g/mol) at 60 °C in Figure II.S4 for the solubility of CO_2 (a), interfacial tension (b), and specific volume of the polyol-rich phase (c). For each property, the measurements made during pressurization (filled symbols) are statistically indistinguishable from those made during depressurization (open symbols), indicating that the measurements were taken near equilibrium, as desired. The one exception is the measurement of the interfacial tension at low pressures in trial 2, which was significantly lower during depressurization than during pressurization. The cause is most likely residual CO_2 because we depressurized the system in larger steps than those with which we pressurized the system, and the CO_2 solubility is slightly higher as well. Therefore, reaching equilibrium would take longer, but due to limited time, we could not always wait to reach equilibrium. The measurements from the two experiments (blue and magenta) are generally indistinguishable, especially those of the specific volume (c).

The primary exception is that the CO_2 solubility was measured to be slightly higher in trial 2 than in trial 1 at pressures above 2000 kPa, which may have resulted in slight variations in the preparation of the sample that were not accounted for in the uncertainty analysis.

II.S2 Estimate Effects of Temperature and Molecular Weight on CO_2 Solubility in 4.7-functional Polyol

In Figure II.5, the solubility of CO_2 in three polyols of similar molecular weight and different functionality is compared. While the CO_2 solubility appears to decrease with increased functionality (from 2f to 3f to 4.7f), the parameters of the measurement for the 4.7-functional polyol are not exactly the same, so a precise comparison cannot be made. Specifically, the 4.7-functional polyol is 25 % shorter than the others, having an average molecular weight of 728 g/mol rather than 1000 g/mol according to the manufacturer (Dow, Inc.). Additionally, the low-temperature measurement of the 4.7-functional polyol was performed at a lower temperature (25 °C) than was that of the other polyols (30.5 °C).

To distinguish the effect of functionality more clearly, we estimated the effects of molecular weight and temperature in this measurement, as shown in Figure II.S5. The effect of temperature can be estimated using a PC-SAFT model, which was developed to model the branched structure of the 4.7-functional polyol. In this branched model, a new species is added to represent the hydroxyl end groups. These are given a high value of the ϵ parameter ($_{OH}$ = 265 k_B) than the backbone ϵ_{bb} = 259 k_B) to model the greater affinity of CO_2 to the backbone than the end groups noted in literature [6]. After fitting the model to the measurements of CO_2 solubility for the 4.7-functional polyol shown in Figure II.5, we used the model to estimate the solubility at 30.5 °C (yellow dashed line in Figure II.S5), which was lower than the solubility measured at 25 °C (yellow circles in Figure II.S5).

To estimate the effect of increasing the molecular weight of the 4.7-functional polyol from the true average value of 728 g/mol to the average value of the 2-functional and 3-functional polyols of 1000 g/mol, we could not use the PC-SAFT model because it does not account for the association of the hydroxyl end groups that leads to the non-monotonic dependence of CO_2 solubility on the molecular weight. Instead, we estimated the effect by extrapolating from the measured increase in Henry's constant based on the data for 2-functional polyols in Figure 3 of the main text, which is reproduced for convenience in Figure II.S6. In the Figure, Henry's

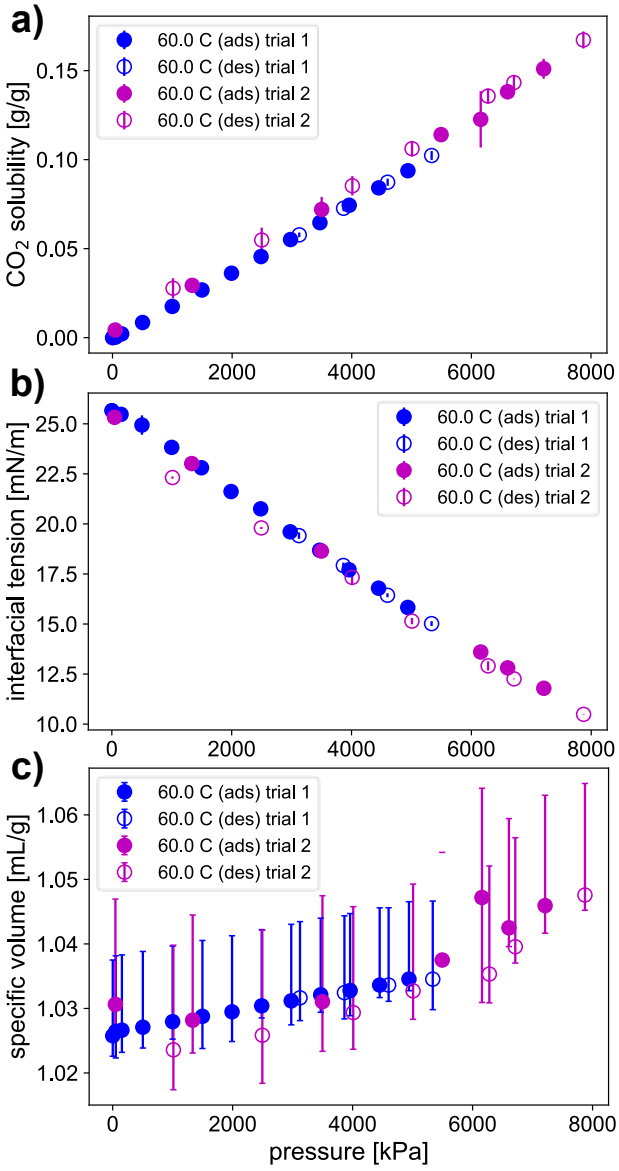

Figure II.S4: Measurements from two experiments of (a) the solubility of CO_2, (b) the interfacial tension, and (c) the specific volume of the polyol-rich phase for a mixture of CO_2 and PPG (2700 g/mol) at 60 °C. Measurements taken during pressurization (adsorption of CO_2) are shown with filled circles while those taken during depressurization (desorption of CO_2) are shown with open circle. The measurements taken from the first trial of the experiment are shown in blue and those taken from the second trial are shown in magenta. Error bars are shown, though they may be smaller than the symbol. In (c), the top error bar represents the systematic error of the experiment while the bottom error bar represents the statistical error of that particular measurement. Measurements are generally statistically indistinguishable, except for the solubility at high pressures and the interfacial tension at lower pressures between experiments.

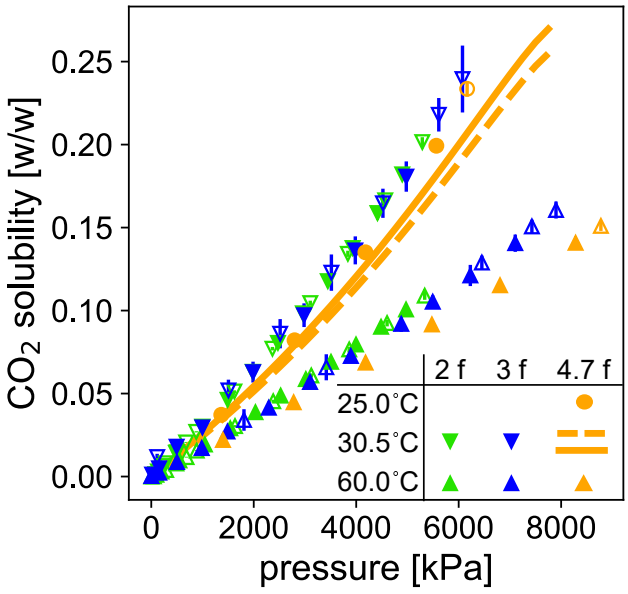

Figure II.S5: Reproduction of Figure II.5 from the main text showing the effect of functionality on the solubility of CO_2 in polyol, here with two estimates of the solubility in a 4.7-functional polyol. The first estimate uses a PC-SAFT model to estimate the effect of increasing the temperature from 25 °C (measurement shown in yellow circles) to 30.5 °C to match the temperature of the low-temperature measurements for the 2-functional and 3-functional polyols (yellow dashed line). The second estimate uses the effect of molecular weight on Henry's constant to estimate the effect of increasing the molecular weight from 728 g/mol (true value) to 1000 g/mol (value for the 2-functional and 3-functional polyols) on Henry's constant at 30 °C, as shown in Figure II.S6, and assumes that the CO_2 solubility would increase by the same fraction (solid yellow line).

constant increases from 0.0260 ± 0.0005 (w/w)/MPa at 400 g/mol to 0.028 ± 0.001 (w/w)/MPa at 1000 g/mol. While a linear interpolation may not be accurate due to the non-monotonicity, the downward concavity of the trendline means that any non-monotonicity would only reduce the increase in Henry's constant with molecular weight from 728 g/mol to 1000 g/mol because Henry's constant at 728 g/mol would be higher.

Therefore, to estimate the largest increase in Henry's constant with molecular weight consistent with the reported measurements, we use a linear interpolation from the lower end of the uncertainty in the measurement at 400 g/mol (0.0255 (w/w)/MPa) to the upper end of the uncertainty in the measurement at 1000 g/mol (0.029 (w/w)/MPa) to estimate a Henry's constant of 0.0274 (w/w)/MPa at 728 g/mol. This linear interpolation is shown in the zoomed-in section of the plot shown in the top of Figure II.S6. The increase in Henry's constant from 728 g/mol to 1000

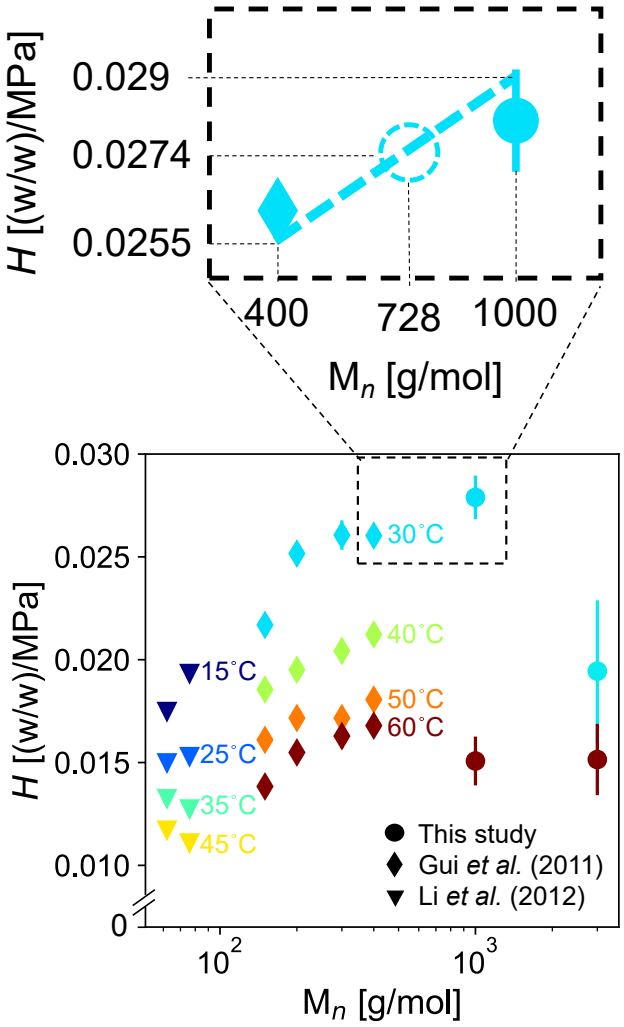

Figure II.S6: Figure II.7 is reproduced at the bottom, showing Henry's constant H in weight fraction of dissolved CO_2 per MPa as a function of number-averaged molecular weight M_n [g/mol]. At the top, the section of the plot used to estimate the effect of molecular weight on Henry's constant at 30 °C between 400 g/mol and 1000 g/mol is shown. As an upper bound on the estimate, the greatest slope within the experimental uncertainty is assumed (dashed blue line). The estimated Henry's constant at 728 g/mol, the molecular weight of the 1k5f polyol, is shown (blue dashed circle). The fractional increase in Henry's constant from 728 g/mol to 1000 g/mol for these 2-functional polyols is used as a rough estimate of the increase in the CO_2 solubility in the 1k5f polyol if its molecular weight were increased from its true value of 728 g/mol to 1000 g/mol. The coordinates of each point on the interpolation line are indicated by thin dashed gray lines.

g/mol would then at most be 0.0274 (w/w)/MPa to 0.029 (w/w)/MPa, which is an increase of 5.8 %. In Figure II.S5, we increased the solubility of CO_2 estimated by the PC-SAFT model at 30.5 °C (yellow dashed line) by 5.8 % as an estimate of

the solubility of CO_2 in a hypothetical 4.7-functional polyol of molecular weight 1000 g/mol at 30.5 °C. These are the identical temperature and molecular weight of the low-temperature measurements of CO_2 solubility in the 2-functional and 3-functional polyols. Even after accounting for the effects of the discrepancy in these parameters in the original measurements shown in Figure 1, we show that our observation that the solubility of CO_2 decrease with functionality still holds.

At 60 °C, the measurements in Figure 3 of the main text show that Henry's constant either stays constant or decreases with molecular weight between 400 g/mol and 1000 g/mol. Therefore, our observation that the solubility of CO_2 decreases with functionality at 60 °C is also still true after accounting for the discrepancy in the molecular weight.

II.S3 Comparison of G-ADSA Measurements to Literature

Here, we show measurements from G-ADSA alongside measurements of the same properties for the same polyols reported in the literature. In Figure II.S7, we compare the measurement of the CO_2 solubility of PPG (2700 g/mol) measured by G-ADSA in the present work and by Near-infrared (NIR) in the work of Guadagno and Kazarian [7]. We note that the solubilities measured with NIR are significantly lower than those measured by G-ADSA, despite the difference in temperature. We expect less statistical error from G-ADSA due to the higher number of measurements at each temperature and the agreement of two repeated experiments (the 60 °C data are combined from two indistinguishable sets of measurements), but we cannot comment on the possibility of unknown sources of systematic error between G-ADSA and the NIR method reported in the literature. Given that Guadagno and Kazarian declare their solubility measurements to be "consistent" with previously published values 30% higher than theirs, we assume that their experimental uncertainty is on the order of 30%. Within this uncertainty, our results are likewise consistent with theirs.

In Figure II.S8, we compare measurements of the solubility of CO_2 in a polyol (three hydroxyls per chain, 1000 g/mol, labeled SD301 in [8]) by G-ADSA from the present work and by a similar method reported by Yang *et al.* [8]. The discrepancy in these measurements is large, with G-ADSA measuring a significantly lower CO_2 solubility at 30.5 °C than Yang *et al.* measured at 35 °C, contrary to our expectation that solubility should decrease with temperature. Both methods use a magnetic suspension balance (Rubotherm) to measure weight and a pendant

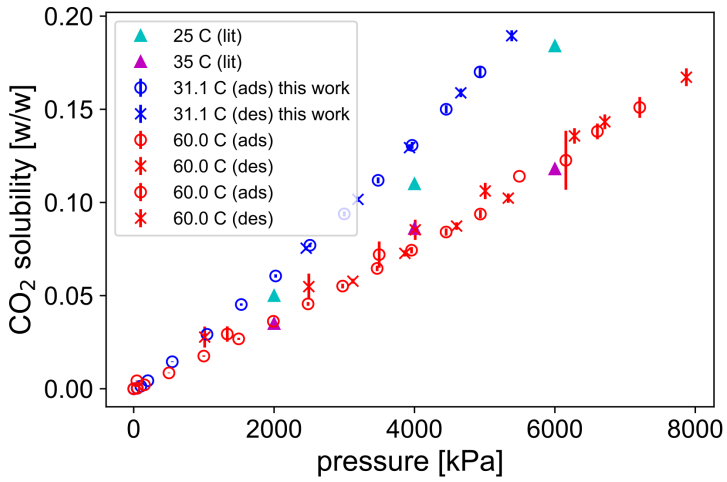

Figure II.S7: Solubility of CO_2 in PPG (2700 g/mol) measured by G-ADSA (○ - adsorption, × - desorption, labeled "this work" in the legend) at 31.1 °C (blue) and 60°C (red) and by FTIR at 25 °C (teal) and 35 °C (purple) by Guadagno and Kazarian [7] (filled triangles, labeled "lit" in the legend).

to measure the interfacial tension. They differ in their estimation of the swelling of the polyol: G-ADSA estimates the swelling by the change in the volume of the pendant drop (assuming axisymmetry) while the method by Yang *et al.* estimates the swelling by the change in the height of the polyol sample in a glass tube (ID = 5 mm). Yang *et al.* repeated their measurements three times, although they applied a much larger change in pressure (2 MPa) between measurements than was used in G-ADSA (≈ 0.5 MPa) and did not perform measurements during depressurization. While Yang *et al.* reported their measurements of solubility in weight of CO_2 per weight of polyol [8], we have converted them to weight of CO_2 per weight of sample for comparison to our measurements. We cannot determine the cause for the significant discrepancy in our results.

We also compared our G-ADSA measurements of the specific volume of this polyol–CO_2 mixture. In this case, the specific volume reported by Yang *et al.* is over 15% higher than the values measured with G-ADSA in the present work. They did not provide a measurement at zero pressure, however, which could have been compared to the value reported in the chemical technical data sheet from Dow (specific gravity of 1.02 at 25 °C, *i.e.* specific volume of 0.98 mL/g). This reported value is consistent with our measurement of a specific volume near 1.00 mL/g at 30.5 °C given that the specific volume increases slightly with temperature. The values reported in the literature at 35 °C exceeded the higher specific volume measured at 60 °C by G-ADSA as well. While each study used a different method to measure

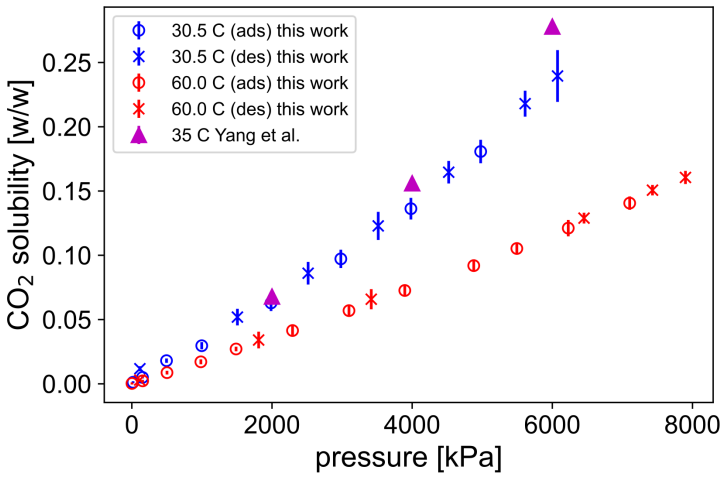

Figure II.S8: Solubility of CO_2 in polyol (three hydroxyls per chain, 1000 g/mol) as a function of pressure measured by G-ADSA and by a similar method reported by Yang *et al.* [8]. G-ADSA data were measured at 30.5 °C (blue) and 60 °C (red). Both adsorption (○) and desorption (×) measurements are shown. Data from Yang *et al.* were measured at 35 °C (cyan filled triangles). Error bars are plotted but may be smaller than glyphs for some data points.

the volume of the sample, we cannot provide an explanation for their significant discrepancy.

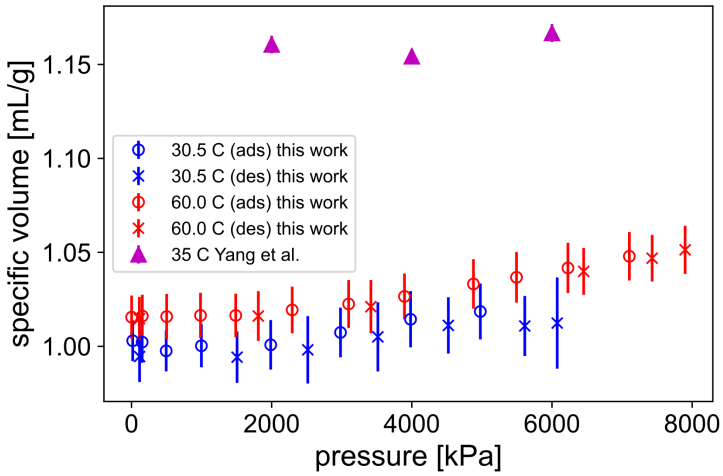

Figure II.S9: Specific volume of a mixture of CO_2 and polyol (three hydroxyls per chain, 1000 g/mol) as a function of pressure measured by G-ADSA and by a similar method reported by Yang *et al.* [8]. G-ADSA data were measured at 30.5 °C (blue) and 60 °C (red). Both adsorption (○) and desorption (×) measurements are shown. Data from Yang *et al.* were measured at 35 °C (cyan filled triangles). Error bars are plotted but may be smaller than glyphs for some data points.

Next we compared our measurements of the diffusivity of CO_2 in this polyol

with G-ADSA to the measurement reported by Yang *et al.* Yang *et al.* estimated the diffusivity using an exponential fit, which we found to be consistent within uncertainty with the square-root fit method (for details on the fit methods, see Section II.S1). Both measurements report a similar power-law increase in diffusivity with pressure. Yang *et al.*, however, report a diffusivity about ten times larger than measured with G-ADSA. While their measurement was performed at a higher temperature (35 °C vs. 30.5 °C with G-ADSA), these diffusivities exceed even those measured at 60 °C by G-ADSA. Nevertheless, we see that an outlier of the G-ADSA data matches the literature data, but we have not explored the cause for this chance agreement.

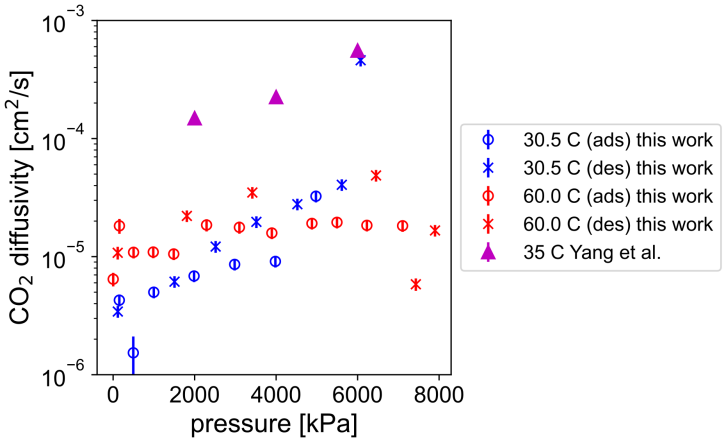

Figure II.S10: Diffusivity of CO_2 in polyol (three hydroxyls per chain, 1000 g/mol) as a function of pressure measured by G-ADSA and by a similar method reported by Yang *et al.* [8]. Both methods fit the transient mass of dissolved gas to an exponential function. G-ADSA data were measured at 30.5 °C (blue) and 60 °C (red). Both adsorption (∘) and desorption (×) measurements are shown. Data from Yang *et al.* were measured at 35 °C (cyan filled triangles). Error bars are plotted but may be smaller than glyphs for some data points.

Last, we compare Henry's constant measured with G-ADSA to measurements for a variety of polyether polyols available in the literature in Figure II.S11. While the data have not been neatly collapsed, a general increase in Henry's constant with molecular weight is observed for M_n < 1000 g/mol followed by a general decrease for M_n > 1000 g/mol. In some studies, solubility data were not provided at low pressures (below 1000 kPa), so we estimated Henry's constant by the slope from the origin to solubility measurement at the lowest pressure.

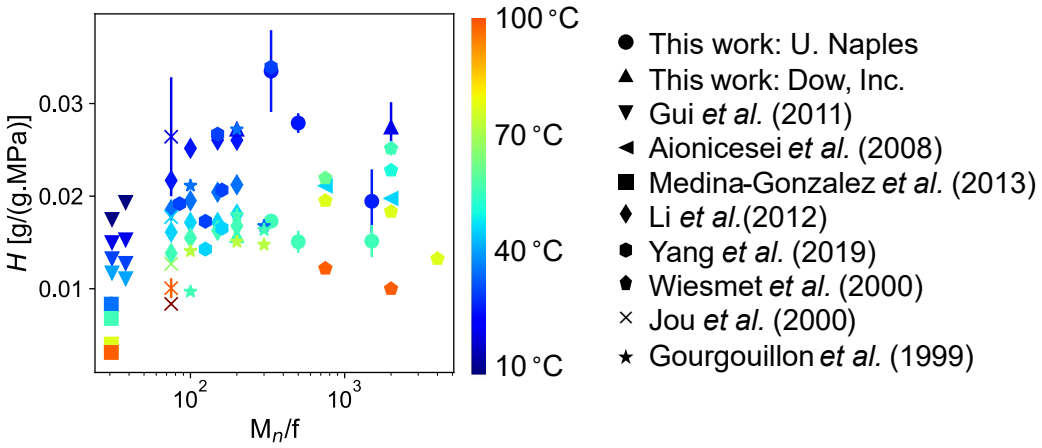

Figure II.S11: Henry's constant for CO_2 solubility in polyether polyols is plotted as a function of the average molecular weight. Both the data measured with G-ADSA in this study and literature data are provided. Error bars may be smaller than glyphs of some data points. Data are shown at different temperatures indicated by the color as defined in the legend.

II.S4 Sensitivity of PC-SAFT and DFT Models to Variations in Parameters

In Section II.4 of the main text, parameters of a PC-SAFT thermodynamic model of the equation of state of a binary mixture of CO_2 and PPG (2700 g/mol) were fit to CO_2 solubility measurements (see Figure II.9). These fitted parameters are reported in Table II.2. Because we fit these parameters through trial and error, we did not compute confidence intervals. Instead, we show the effect of ±5% variations in each of these parameters on the predictions of different properties made by the PC-SAFT (for specific volume and solubility) and corresponding DFT (for interfacial tension) models in Figure II.S12.

The properties of the polyol–CO_2 mixture are most sensitive to the polyol bead size σ, as seen in the left column of Figure II.S12. CO_2 solubility increases with bead size while interfacial tension decreases, in large part due to the increased concentration of dissolved CO_2. The specific volume increases with bead size since the molecular weight of each bead is kept the same, but interestingly the effect of pressure on the specific volume reverses. For small bead size (σ = 2.86 Å, blue line), the specific volume increases with pressure, while at large bead size (σ = 3.16 Å, red line), the specific volume decreases with pressure. Interestingly, the best quantitative agreement with the G-ADSA measurements is achieved with the large bead size, while the best qualitative agreement with the general increase in specific volume with pressure is achieved with the small bead size. We expect that a different model is needed to achieve both quantitative and qualitative agreement, likely one

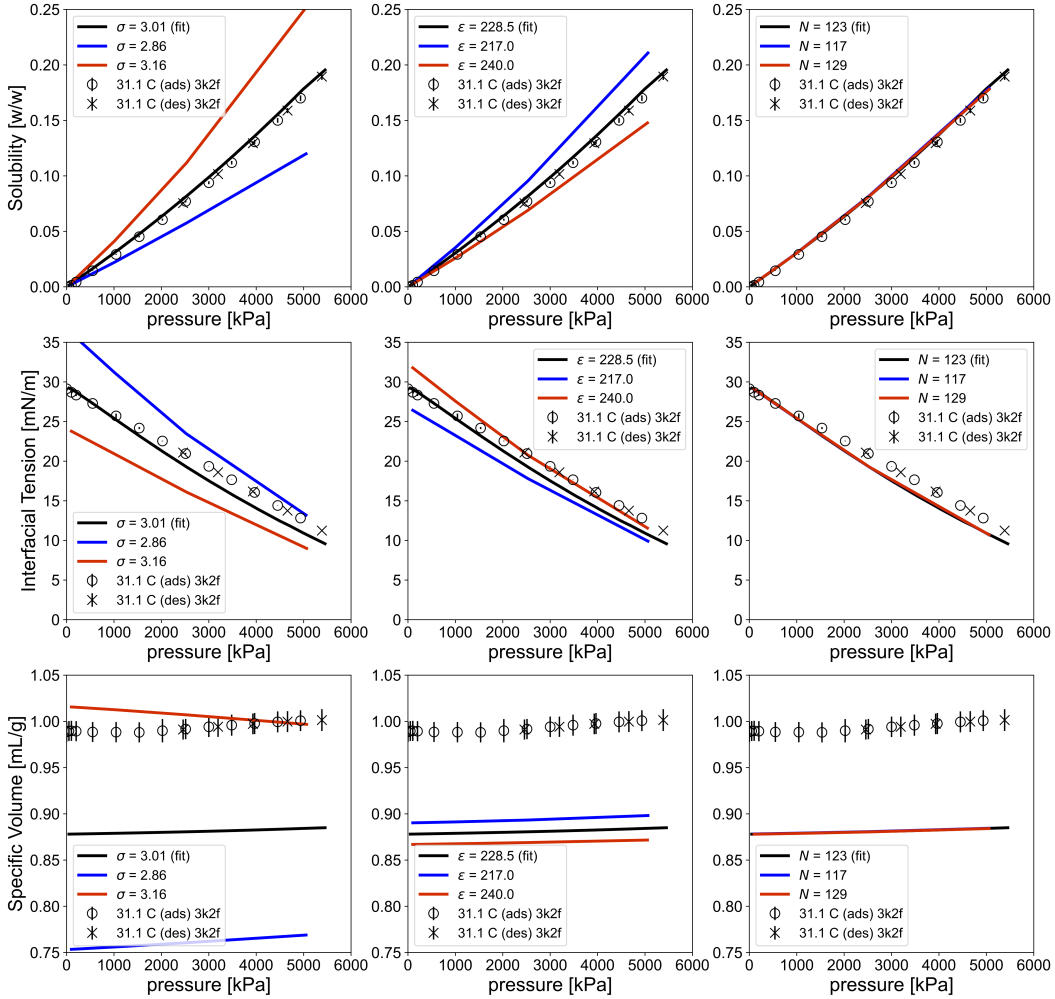

Figure II.S12: The sensitivity of the predictions of our PC-SAFT and DFT models to the polyol parameters σ (bead size, Angstroms, first column), ε (energy parameter, k_B, second column), and N (number of beads, third column) to +5% (red) and -5% (blue) variations about the fitted value (black) are plotted for the solubility of CO_2 (first row, PC-SAFT), interfacial tension (second row, DFT), and specific volume (third row, PC-SAFT) of a mixture of CO_2 and PPG (2700 g/mol). The G-ADSA data measured at 31.1 °C are shown in black (adsorption ∘ and desorption ×). Error bars may be smaller than glyphs for some data points.

that accounts for the association interactions of hydrogen bonding.

The effect of the polyol bead interaction strength ϵ on the polyol–CO_2 properties is smaller and opposite the effect of σ, as seen in the center column of Figure II.S12. Because their effects are opposite, ϵ can be varied to "cancel out" the effect of varying σ, such that the same predictions for solubility and interfacial tension are made for a degenerate set of pairs of σ and ϵ. The effect on specific volume is not entirely opposite, however, because varying ϵ has a negligible effect

on the qualitative behavior of the specific volume with pressure and the quantitative effect of varying σ is significantly more than that of varying ϵ. Consequently, within this degenerate set of pairs of σ and ϵ, the predictions for specific volume can be adjusted while those for solubility and interfacial tension remain the same.

Finally, the effect of the molecular weight is negligible on the scale of 5% variations, as seen in the far right column of Figure II.S12. The model predictions for each value of N are almost indistinguishable at the scale at which they are shown. We believe that the reason for the small size of the effect of N is that its primary contribution to the free energy comes into the translational entropy of the polymer, which is proportional to $1/N$. At $N = 123$, a 5% change in N yield a roughly 5% change in $1/N$, which is already small. We expect that a significant decrease in N would increase the translational entropy of the polymer and drive greater mixing, *i.e.* greater solubility of CO_2 given that the CO_2-phobicity of the hydroxyl end groups is not accounted for in this model.

Alternative Parameters Increase Predicted Specific Volume, Leave Solubility and Interfacial Tension Unchanged

Given that the PC-SAFT model grossly underestimated the specific volume (see Figure II.12), we explored other model parameters that deviated more from the predictions of the group contribution method [9]. We found that by increasing both bead size σ and the interaction energy ϵ in proportion, we could increase the estimate for the specific volume to be closer to the experimental measurement without changing the estimates for solubility or interfacial tension.

II.S5 DFT Predicts Non-monotonic CO_2 Concentration Profile

In the main text, we only discuss the interfacial tension along the vapor–liquid interface predicted by our DFT model. This interfacial tension is computed from a complete density profile along the interface. An example of such a density profile predicted by our DFT model is shown in Figure II.S14. The plot shows the concentrations of CO_2 and PPG (2700 g/mol) at the interface between the CO_2-rich (left) and polyol-rich (right) phases. Interestingly, the CO_2 partitions similarly in both phases but accumulates at the interface. Such behavior is reminiscent of a surfactant and suggests that CO_2 may condense at the surface of bubbles that form at high pressure to mediate the drastic change in density from polyol-rich liquid to CO_2-rich vapor. This non-monotonic density profile of the volatile component was predicted with DFT for a binary mixture of liquid and gas by Talanquer and Oxtoby

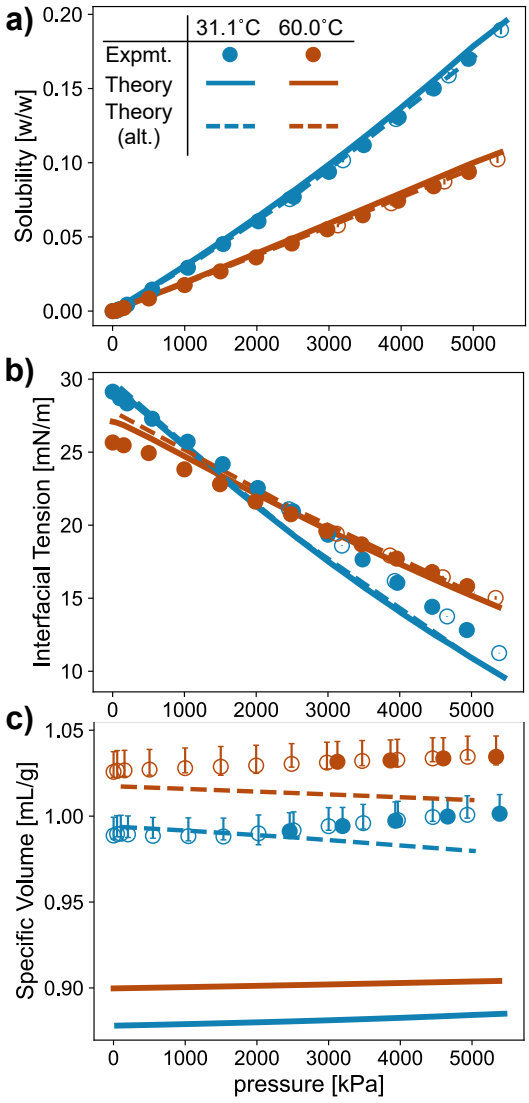

Figure II.S13: The agreement between the PC-SAFT model and measurements of a mixture of CO_2 and 2700 g/mol PPG is shown for two sets of PC-SAFT parameters. The predictions of the model using the parameters listed in Table II.2 is plotted in solid lines. The predictions of the model using σ = 3.17 Åand ϵ = 253 k_B for the polyol (same N value) are shown with dashed lines (alternative theory). Data are plotted as a function of pressure [kPa] for two temperatures, 31.1 °C (blue) and 60 ° (red). a) Solubility of CO_2 [w/w] in polyol. b) Interfacial tension between polyol-rich and CO_2-rich phases [mN/m]. c) Specific volume of polyol-rich phase. The models are identical except in their prediction of the specific volume, for which the model represented by the solid line accurately models the qualitative trend but is inaccurate quantitatively while the model represented by the dashed line (alternative) is more quantitatively accurate but predicts the opposite qualitative trend with pressure.

[10] as well as for a binary mixture of CO_2 and PMMA [11–13] and CO_2 and P(MMA-*co*-EA) copolymer [14]. Talanquer and Oxtoby attribute the decrease in

the interfacial tension with pressure predicted by DFT (see Fig. II.11) to the increase in the amount of this enrichment of the volatile component along the liquid–vapor interface.

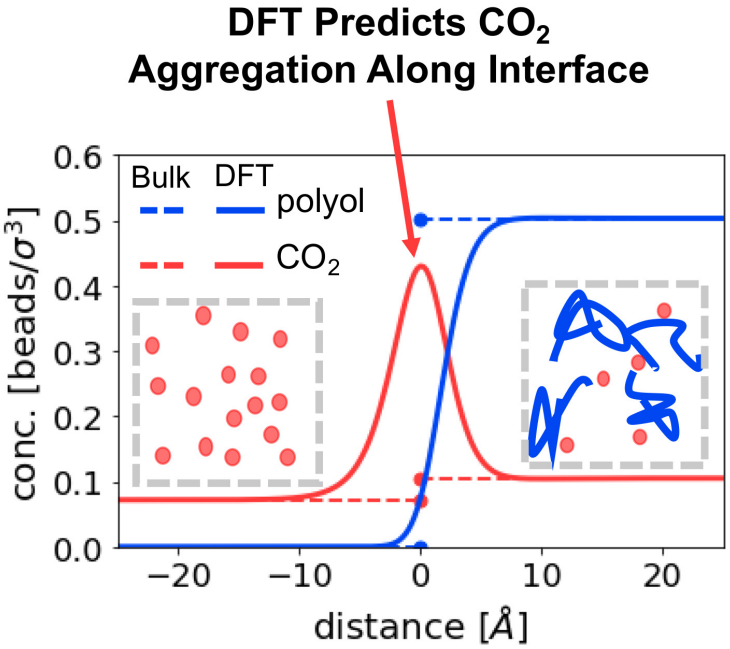

Figure II.S14: Density profiles of CO_2 and PPG (2700 g/mol) at the interface between CO_2-rich (< 100 Å) and polyol-rich (> 100 Å) phases at 5 MPa and 31 °C. Note that CO_2 has a similar partitioning in both phases but accumulates at the interface.

References

1. Ylitalo, A. S. *andylitalo/g-adsa: v0.1.0* 2022. https://github.com/andylitalo/g-adsa (2022).
2. NIST. *NIST Standard Reference Database Number 69* 2022. https://webbook.nist.gov/chemistry/ (2022).
3. Pastore Carbone, M. G., Di Maio, E., Iannace, S. & Mensitieri, G. Simultaneous experimental evaluation of solubility, diffusivity, interfacial tension and specific volume of polymer/gas solutions. *Polymer Testing* **30,** 303–309. ISSN: 01429418. https://linkinghub.elsevier.com/retrieve/pii/S0142941811000067 (May 2011).
4. Crank, J. *The Mathematics of Diffusion* 2nd Ed., 1–352 (Oxford University Press, London, 1975).
5. Song, B. & Springer, J. Determination of interfacial tension from the profile of a pendant drop using computer-aided image processing. *Journal of Colloid and Interface Science* **184,** 64–76. ISSN: 00219797 (1996).

6. Parks, K. L. & Beckman, E. J. Generation of microcellular polyurethane foams via polymerization in carbon dioxide. I: Phase behavior of polyurethane precursors. *Polymer Engineering & Science* **36,** 2404–2416. ISSN: 0032-3888. https://onlinelibrary.wiley.com/doi/10.1002/pen.10639 (Oct. 1996).

7. Guadagno, T. & Kazarian, S. G. High-Pressure CO 2 -Expanded Solvents: Simultaneous Measurement of CO 2 Sorption and Swelling of Liquid Polymers with in-Situ Near-IR Spectroscopy. *The Journal of Physical Chemistry B* **108,** 13995–13999. ISSN: 1520-6106. https://pubs.acs.org/doi/abs/10.1021/jp0481097%20https://pubs.acs.org/doi/10.1021/jp0481097 (Sept. 2004).

8. Yang, Z. *et al.* Effect of the properties of polyether polyol on sorption behaviour and interfacial tension of polyol/CO2 solutions under high pressure condition. *The Journal of Chemical Thermodynamics* **133,** 29–36. ISSN: 00219614. https://linkinghub.elsevier.com/retrieve/pii/S0021961419300643 (June 2019).

9. Tihic, A., Kontogeorgis, G. M., von Solms, N., Michelsen, M. L. & Constantinou, L. A Predictive Group-Contribution Simplified PC-SAFT Equation of State: Application to Polymer Systems. *Industrial & Engineering Chemistry Research* **47,** 5092–5101. ISSN: 0888-5885. https://pubs.acs.org/doi/10.1021/ie0710768 (Aug. 2008).

10. Talanquer, V. & Oxtoby, D. W. Nucleation of bubbles in binary fluids. *The Journal of Chemical Physics* **102,** 2156–2164. ISSN: 0021-9606. http://aip.scitation.org/toc/jcp/102/5%20http://aip.scitation.org/doi/10.1063/1.468737 (Feb. 1995).

11. Xu, X., Cristancho, D. E., Costeux, S. & Wang, Z.-G. Bubble nucleation in polymer–CO2 mixtures. *Soft Matter* **9,** 9675. ISSN: 1744-683X. www.rsc.org/softmatter%20http://xlink.rsc.org/?DOI=c3sm51477c (2013).

12. Xu, X., Cristancho, D. E., Costeux, S. & Wang, Z.-G. Density-functional theory for polymer-carbon dioxide mixtures: A perturbed-chain SAFT approach. *The Journal of Chemical Physics* **137,** 054902. ISSN: 0021-9606. http://aip.scitation.org/doi/10.1063/1.4742346 (Aug. 2012).

13. Xu, X., Cristancho, D. E., Costeux, S. & Wang, Z.-G. Discontinuous Bubble Nucleation Due to a Metastable Condensation Transition in Polymer–CO2 Mixtures. *The Journal of Physical Chemistry Letters* **4,** 1639–1643. http://pubs.acs.org/doi/10.1021/jz4005575 (May 2013).

14. Xu, X., Cristancho, D. E., Costeux, S. & Wang, Z.-G. Density-Functional Theory for Mixtures of AB Random Copolymer and CO 2. *Macromolecules* **48,** 6035–6046. ISSN: 0024-9297. https://pubs.acs.org/doi/10.1021/acs.macromol.5b01122 (Aug. 2015).